UC Santa Cruz
UC Santa Cruz Electronic Theses and Dissertations

Title
Characterization Of High-Stroke High-Aspect Ratio Micro Electro Mechanical Systems Deformable Mirrors For Adaptive Optics

Permalink
https://escholarship.org/uc/item/26h990mc

Author
Bouchti, Mohamed Amine

Publication Date
2013

Peer reviewed|Thesis/dissertation

eScholarship.org Powered by the California Digital Library
University of California

UNIVERSITY OF CALIFORNIA

SANTA CRUZ

Characterization Of High-Stroke High-Aspect Ratio Micro Electro Mechanical Systems Deformable Mirrors For Adaptive Optics

A thesis submitted in partial satisfaction
of the requirements for the degree of

MASTER OF SCIENCE

in

ELECTRICAL ENGINEERING

by

Mohamed Amine Bouchti

June 2013

The Thesis of Mohamed Amine Bouchti
is approved:

____
Professor Joel A. Kubby, Chair

____
Professor Nobuhiko Kobayashi

____
Don Gavel, Director of the Laboratory for
Adaptive Optics, UCSC

____
Tyrus Miller
Vice Provost and Dean of Graduate Studies

Copyright © by
Mohamed Amine Bouchti
2013

Table of Contents

List of Figures v

List of Tables ix

Abstract x

Dedications xii

Acknowledgement xiii

Chapter 1: Introduction 1

- 1.1 Introduction 1
- 1.2 MEMS Actuators 3
- 1.3 Deformable Mirror Fabrication 8
- 1.4 X-Beam Design 12

Chapter 2: Deformable Mirror Testing 16

- 2.1: Actuator Packaging and PCB Test Board 16
- 2.2: WYKO Interferometer 20
- 2.3: Testing Procedure 22

Chapter 3: Deformable Mirror Testing Results 29

- 3.1: Challenges 29
- 3.2: Results 36
  - 3.2.1: Individual Actuator Testing 37
  - 3.2.2: Two-Actuators Testing 39

3.3: Summary/Discussion 46

Chapter 4: Future Work 54

4.1: Individual Actuator Testing 54

4.2 Dual Actuator Testing 57

4.3: Future work 61

Chapter 5: Conclusion 63

Bibliography 64

List of Figures

Figure 1.1: Schematic of parallel light Rays (Left) vs. rays affected by turbulence 1

Figure 1.2: Schematic of adaptive optics system 2

Figure 1.3: Shack Hartman wavefront sensor 2

Figure 1.4: Parallel plate actuator mode 3

Figure 1.5: Monolithic fabrication process overview. (A) Patterning, electroplating, and CMP of counter electrodes and anchor post. (B) Patterning, electroplating, and CMP of the spring layer. (C) Patterning, electroplating, and CMP of the mirror support post and of the mirror layer. (D) Released continuous facesheet mirror attached to actuators 9

Figure 1.6: 3D actuator designs modeled with FEA. (A) Square actuators supported by eight folded springs at the corners. (B) Circular actuators supported by four folded springs. (C) X-beam actuators supported by four fixed-guided beams 11

Figure 1.7: The three actuator's designs shown in Figure 1.6 fabricated out of gold 12

Figure 1.8: Fixed-fixed beam subjected to a point load F at the middle of the beam 13

Figure 1.9: layout of 16x16 deformable mirror array 15

Figure 1.10: Close-up view of the top right of a 16x16 deformable mirror array 15

Figure 2.1: Packaged Deformable Mirror 16

Figure 2.2: PCB layout for 16x16 deformable mirror 17

Figure 2.3: Location of the center 4x4 Actuator of the deformable mirror in the ZIF Socket 18

Figure 2.4: ZIF Socket Mounted on the fabricated PCB 19

Figure 2.5: represents the flow chart of the VSI algorithm used to extract the interference signal 20

Figure 2.6: Schematic representation of the Veeco WYKO interferometer 21

Figure 2.7: Image of the WYKO interferometer used for testing the deformable mirrors 21

Figure 2.8: Fringes of the deformable mirror 23

Figure 2.9: Surface Scan of a deformable mirror before alignment 24

Figure 2.10: Surface Scan of a deformable mirror after alignment 24

Figure 2.11: Window for setting the maximum slope and minimum islands 25

Figure 2.12: Window for defining the actuators of interests and references 26

Figure 2.13: Window after finishing the set up and calculating the initial heights of the actuators of interest 27

Figure 2.14: Database view and graphs of displacement vs. voltage for dual actuator testing. 28

Figure 3.1: Displacement vs. voltage for a 10x10 mirror system 29

Figure 3.2: Oscillating behavior in the Displacement vs. voltage graph for a dual actuator-system testing 31

Figure 3.3: Probe station used for electrical and mechanical probing 32

Figure 3.4: ZIF socket pin array. Blue dots represent the pins wanted. Red dots represent the pins obtained 32

Figure 3.5: DM Packaging. Blue lines represent the pins wanted. Red lines represent the pins obtained 33

Figure 3.6: Layout of the Horizontally flipped PCB 33

Figure 3.7: Correct orientation of the mirror with respect to packaging 34

Figure 3.8: 90 degrees CCW rotation of the mirror with respect to packaging 34

Figure 3.9: 90 degrees CW rotation of the mirror with respect to packaging 35

Figure 3.10: Center 4 x 4 actuators of the deformable mirror with the hole in the top 36

Figure 3.11: Graph of voltage vs. displacement for actuator (7,7) 37

Figure 3.12: Graph of voltage vs. displacement for actuator (10,7) 38

Figure 3.13: Graph of voltage vs. displacement for actuator (10,8) 38

Figure 3.14: Trial 1 for dual actuator testing for actuator (7,7) and (7,8) 39

Figure 3.15: Trial 2 for dual actuator testing for actuator (7,7) and (7,8) 40

Figure 3.16: Trial 3 for dual actuator testing for actuator (7,7) and (7,8) 40

Figure 3.17: Trial 1 for dual actuator testing for actuator (10,7) and (10,8) 41

Figure 3.18: Trial 2 for dual actuator testing for actuator (10,7) and (10,8) 42

Figure 3.19: Trial 3 for dual actuator testing for actuator (10,7) and (10,8) 42

Figure 3.20: Trial 4 for dual actuator testing for actuator (10,7) and (10,8) 43

Figure 3.21: Repeatability of actuator (7,7) throughout the 3 trials 44

Figure 3.22: Repeatability of actuator (7,8) throughout the 3 trials 44

Figure 3.23: Repeatability of Actuator (10,7) throughout the four trials 45

Figure 3.24: Repeatability of Actuator (10,7) throughout the four trials 45

Figure 3.25: Height of actuators located in the corner of the deformable mirror as well as the height of actuators in the middle of each side of the mirror 48

Figure 3.26: Average height from the substrate to the mirror layer, from the substrate to the spring layer and for the counter electrode of this deformable mirror 49

Figure 3.27: An illustration of a test-structure (bulls-eye) found around the mirror 50

Figure 3.28: Standard Paschen curve, modified Paschen curve, Vacuum breakdown, and safe operating region for MEMS for air at one atmosphere 53

Figure 4.1: Image of the Center 4 x 4 X-Beam Actuators 54

Figure 4.2: Graph of the average displacement of actuator (7,7), (8,7) and (10,7) from 0 to 280 V for the top row of the center 4 x 4 55

Figure 4.3: Graph of the average displacement of actuator (8,8), (9,8) and (10,8) from 0 to 280 V for the second row of the center 4 x 4 55

Figure 4.4: Graph of the average displacement of actuator (7,9), (8,9), (9,9) and (10,9) from 0 to 280 V for the third row of the center 4 x 4 56

Figure 4.5: Graph of the average displacement of actuator (7,10), (8,10), and (9,10) from 0 to 280 V for the bottom row of the center 4 x 4 56

Figure 4.6: Repeatability of Actuator (7,7) throughout the four Trials of dual actuator testing of the second DM 57

Figure 4.7: Repeatability of Actuator (7,8) throughout the four Trials of dual actuator testing of the second DM 58

Figure 4.8: Repeatability of Actuator (7,9) throughout the four Trials of dual actuator testing of the second DM 58

Figure 4.9: Repeatability of Actuator (7,10) throughout the four Trials of dual actuator testing of the second DM 59

Figure 4.10: Repeatability of Actuator (8,7) throughout the four Trials of dual actuator testing of the second DM 59

Figure 4.11: Repeatability of Actuator (8,8) throughout the four Trials of dual actuator testing of the second DM 60

Figure 4.12: Repeatability of Actuator (8,9) throughout the four Trials of dual actuator testing of the second DM 60

Figure 4.13: Repeatability of Actuator (8,9) throughout the four Trials of dual actuator testing of the second DM 61

List of Tables

Table 2.1: The Die pad name, Die pad number and the equivalent package pad number of the center 4x4 actuators 18

Table 3.1: The maximum displacement of actuators (7,7) and (7,8) in pair actuator testing in all trials 46

Table 3.2: The maximum displacement of actuators (10,7) and (10,8) in pair actuator testing in all trials 46

Table 3.3: Comparison of the displacement between single and dual actuation for each actuator 47

Table 3.4: Summary of the heights of the counter electrode, the gap between the counter electrode and spring layer, the post gap, the mirror layer and the total height of each bulls-eye that are part of the DM. 50

Table 3.5: Summary of the heights of the counter electrode, the gap between the counter electrode and spring layer, the post gap, the mirror layer and the total height of bulls-eyes that are not part of the 51

Table 3.6: Comparison between the heights of the counter electrode, the gap between the counter electrode and spring layer, the post gap, the mirror layer and the total height of bulls-eyes that are part of the DM and ones that are not part of the DM. 52

Abstract

Characterization Of High-Stroke High-Aspect Ratio Micro Electro Mechanical Systems Deformable Mirrors For Adaptive Optics

Mohamed Amine Bouchti

Adaptive optics MEMS deformable mirror, in conjunction with Shack Hartman wave front sensor and real-time controller, is capable of correcting time-varying aberrations in imaging applications through manipulating its mirror surface. Adaptive optics systems in astronomy for next generation large telescopes (30 meter primary mirrors) require a high stroke of 10μm of mechanical displacement. This required stroke would be achieved by MEMS deformable mirrors fabricated with high aspect ratio techniques.

This thesis will review the designs of various types of high aspect actuators consisting of folded springs with rectangular and circular membranes as well as X-beam actuators. Finite element analysis (FEA) simulations of these designs have shown the ability of each design to achieve a stroke of approximately 9.4 μm. Also, FEA simulations proved that the X-beam actuators provide the best spring support while preventing tilting.

In addition, this thesis will discuss device characterization and voltage vs. displacement test results for the high aspect ratio gold MEMS 16 x 16 X-beam

actuators deformable mirror that has been bonded and packaged. The results have shown that the device is capable of achieving approximately 5.5 μm in individual actuator testing and 7μm in dual actuator testing.

To my parents Bouchti Ahmed and Moutawakkil Halima,
to my sisters and my brother Laila, Tarik and Hanane Bouchti
to my wife Josie and her dad Richard Moss
to my brother-in-law Richard King and my Friend Erin McGinty.

Acknowledgements

I would like to thank my research advisor Dr. Joel A. Kubby for his support and guidance and the other members of my committee, Dr. Donald T. Gavel and Dr. Nobuhiko Kobayashi. I would also thank the Initiative for Maximizing Student Diversity (IMSD) funded through NIGMS, NIH for giving me the opportunity and the support during my first two years of graduate school.

I would like to thank Baustista Fernandez for his support and guidance. I would also like to thank my family, my wife and friends for their love, support and encouragement that allowed me to be at this stage of my life.

I would also like to thank the MEMS Research Laboratory group at UC Santa Cruz, especially, Dmitry Medved, Oscar Azucena, Zachary Graham, Andrew Norton, Dan O'Leary, Marco Reinig, and Xiaodong Tao for taking the time to attend my presentations and provide me with valuable feedbacks.

Chapter 1: Introduction

1.1 Introduction

Adaptive optics (AO) MEMS deformable mirrors (DM) are used in astronomy in order to improve the performance of optical systems by compensating for aberrations due to fabrication errors, thermal fluctuations and atmospheric turbulence. Plane waves passing through the atmosphere encounter temperature fluctuations in small patches of air causing changes in index of refractions. This flux of index of refraction causes light to refract many times by small amounts leading to skew rays. Hence, the rays can't be focused to a point as shown in figure (1.1) below causing a distorted wavefront and therefore a blurry image [1] [3] [4].

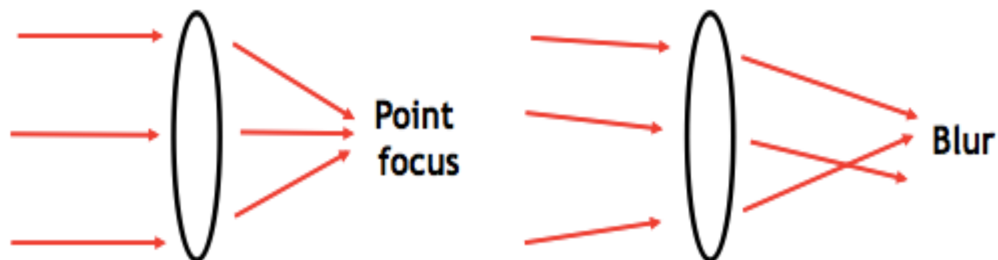

Figure 1.1: Schematic of parallel light Rays (Left) vs. rays affected by turbulence [1]

The main components of an AO system, as shown in figure (1.2), are a wavefront sensor, a control system and a deformable mirror. Shack-Hartman wavefront sensor (SHWFS) is used to measure the distorted wavefront. This sensor splits light into a number of small beams using an array of miniature lenses, called lenslets. The light from each of these lenslets is focused onto a CCD camera as shown in figure (1.3) below. As the portion of the wavefront hitting the lenslet is aberrated, the focused spot on the CCD camera moves. Through simple geometry using the displacement of the focused spot and the focal length of the lenslet, the local tilt of the wavefront is approximated [1] [2] [9].

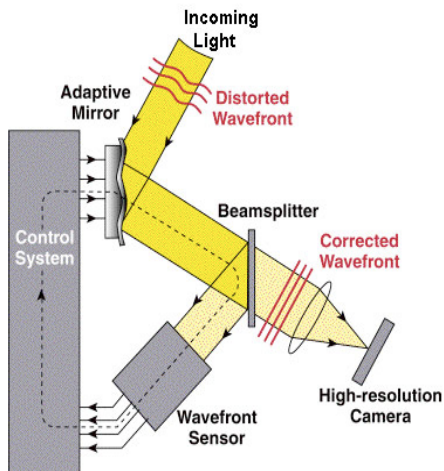

Figure 1.2: Schematic of adaptive optics system [1]

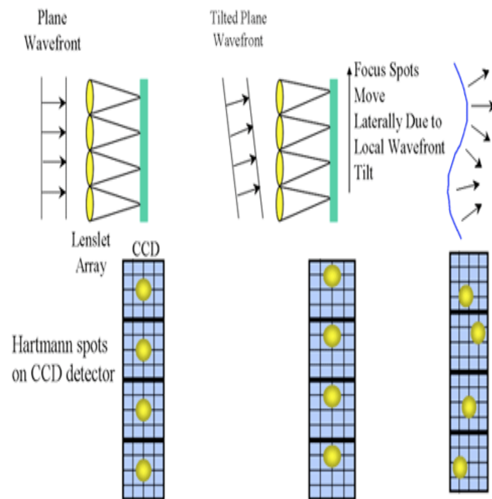

Figure 1.3: Shack Hartman wavefront sensor [2]

Once the wavefront is measured, a control system (typically a computer running control algorithm software) calculates the appropriate shape needed to compensate the wavefront and sends that information to the deformable mirror. The deformable mirror changes the spatial phase of a wavefront using an array of actuators that deforms the mirror's surface. The appropriate shape of the mirror to compensate for each aberration is simply the same shape as the wavefront with half the amplitude since the reflection doubles the effect [1] [2].

1.2 MEMS Actuators

The actuators of the deformable mirrors are electrostatically actuated and move in a piston like motion. Each actuator is modeled as a two parallel-plate capacitor with gap g between them, area A and dielectric constant ε. The top plate is connected to a spring and it is free to move, while the bottom plate is fixed to the substrate as shown in figure (1.4). Applying a voltage V results in an attractive electrostatic force F_e that bends the actuator membrane downward.

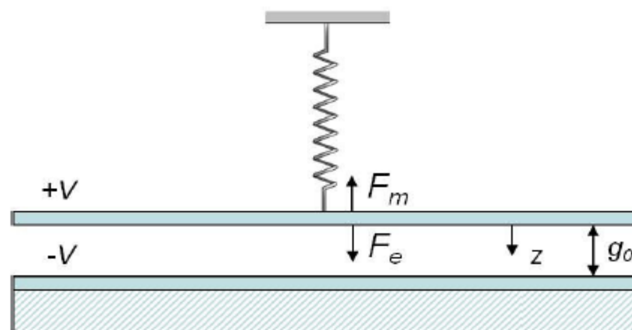

Figure 1.4: Parallel plate actuator mode [3]

This electrostatic force is related to the mechanical work done from the outside in moving the plate by a distance Z, which is given by equation (1.1):

$$\Delta W = F_e \cdot \Delta Z \qquad (1.1)$$

While the electric work, if we control the voltage and let charge flow into the capacitor from a battery, is given by equation (1.2):

$$\Delta W_e = \Delta q \cdot V = \left(V \cdot \Delta C\right) \cdot V = V^2 \cdot \Delta C \qquad (1.2)$$

In addition, the work required in charging the capacitor due to a change in charge Q at constant voltage is given by equation (1.3) as follow:

$$dU = V \cdot dq$$

$$dU = \frac{Q}{C} \cdot dq \quad \text{where } \mathrm{Q} = \mathrm{C} \cdot V$$

$$U = \int \frac{Q}{C} \cdot dq = \frac{1}{2} \cdot \frac{Q^2}{C}$$

$$U = \frac{1}{2} C \cdot V^2 \qquad (1.3)$$

The electrostatic force is found by balancing the change in the potential energy in the capacitors with the sum of the mechanical work and the electric work as follows:

$$\Delta U_{Capacitor} = \Delta W_{Mechanical} + \Delta W_{Electrical}$$

$$\frac{1}{2}V^2 \cdot \Delta C = F_e \cdot \Delta Z + V^2 \cdot \Delta C$$

$$-\frac{1}{2}V^2 \cdot \Delta C = F_e \cdot \Delta Z$$

$$F_e = -\frac{1}{2}V^2 \cdot \frac{\Delta C}{\Delta Z} \qquad (1.4)$$

The capacitance of the parallel plates is given by the (1.5):

$$C = \frac{\varepsilon \cdot A}{g_0 - z} \quad \text{where} \quad g = g_0 - z \qquad (1.5)$$

And therefore the electrostatic force becomes:

$$F_e = -\frac{1}{2}V^2 \cdot \frac{dC}{dz}$$

$$F_e = -\frac{1}{2}V^2 \cdot \frac{d}{dz}\left(\frac{\varepsilon \cdot A}{g_0 - z}\right)$$

$$F_e = -\frac{1}{2}V^2 \cdot \left(\frac{-\varepsilon \cdot A}{\left(g_0 - z\right)^2}\right)$$

$$F_e = \frac{1}{2}\frac{\varepsilon \cdot A \cdot V^2}{\left(g_0 - z\right)^2} \tag{1.6}$$

On the other hand, a linear spring is used to apply a mechanical restoring force F_m for electrostatic actuators that can be expressed in equation (1.7) as follow:

$$F_m = -k \cdot z \tag{1.7}$$

Where k is the spring constant and z is the distance the spring either stretched or compressed.

One of the limitations of the deformable mirror is that the displacement of electrostatic actuators is stable only up to 1/3 of the gap between the plates. Once the displacement exceeds this threshold the mechanical force becomes larger than the electrostatic force and the actuator membrane snaps-in unstably into the fixed plate [3]. Therefore, it is very important to calculate the maximum voltage V_{pi} that can be applied before a pull-in occurs. At this voltage, equilibrium is established where the electrostatic force and mechanical force are equal. Therefore, the V_{pi} can be calculated as follow:

$$F_e = F_m$$

$$\frac{1}{2}\frac{\varepsilon \cdot A \cdot V}{\left(g_0 - z\right)^2} = -k \cdot z$$

Solving for V as a function of Z we get:

$$V = \sqrt{\frac{2 \cdot k \cdot z \cdot (g_0 - z)}{\varepsilon \cdot A}}$$

And evaluating z at 1/3 of the gap leads to the pull-in voltage given by equation (1.7)[3]:

$$V = \left. \sqrt{\frac{2 \cdot k \cdot z \cdot (g_0 - z)}{\varepsilon \cdot A}} \right|_{z=\frac{g_0}{3}}$$

$$V_{pi} = \sqrt{\frac{8 \cdot k \cdot g_0^3}{27 \cdot \varepsilon \cdot A}} \qquad (1.8)$$

1.3 Deformable Mirror Fabrication

Adaptive optics applications in astronomy require a high stroke of 10μm of mechanical displacement. However, current deformable mirrors are fabricated using surface micromachining techniques that provide only a stroke of less than 6μm for continuous-facesheet mirrors. Commercial MEMS deformable mirrors developed by Boston Micromachines Corporation provide a stroke between 1.5 to 5.5μm. This limitation is due to the fact that the sacrificial oxide layer in the surface micromachining process is limited to a thin-film of 2μm [4].

Dr. Kubby and Dr. Fernandez have fabricated deformable mirrors with MEMS high-stroke actuators using high aspect ratio Innovative Micro Technologies (IMT). IMT uses a monolithic fabrication process that allows for thick layer deposition, between 10 to 100μm, of sacrificial layer and therefore allowing for a 10μm stroke required for astronomical applications [5].

This process is performed on optically flat WMS-15 glass-ceramic substrates with thermal expansion of 11.4 x 10^{-6} K^{-1} (close to the coefficient of thermal expansion of gold, which is 14.2 x 10^{-6} K^{-1}) and involves four phases. The first phase, as shown in figure (1.5a), in the fabrication starts with a deposition, a lift off and then a patterning of a 0.5μm electrode layer on the substrate. The next step is the patterning and electroplating of the gold actuator anchors to a height of 22μm. The electroplated gold anchors and copper sacrificial layer are planarized down to a height of approximately 20μm with a chemical mechanical

planarization (CMP) process. The next phase involves the patterning and electroplating of a 4μm gold spring layer followed by a copper electroplating up to the height of the spring layer. In addition, these layers undergo CMP planarization as shown in figure (1.5b). The third phase incorporates 30μm of patterned and electroplated mirror support posts and an electroplated copper sacrificial layer. Once again, the electroplated mirror post and the sacrificial layer are planarized using CMP as shown in figure (1.5c). In addition, a 2μm gold mirror layer is patterned electroplated and then planarized to an optical mirror. And finally, a chemical etching step is required to remove the copper sacrificial layer resulting in an approximately 56.5μm high released structure as illustrated in figure (1.5d) [4] [5].

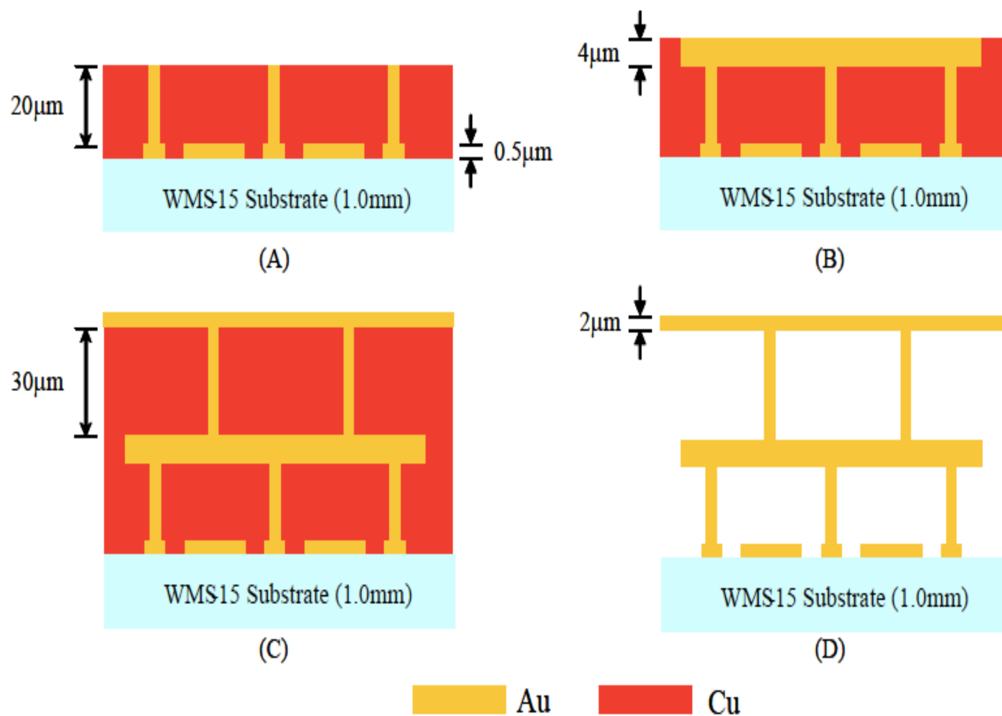

Figure 1.5: Monolithic fabrication process overview. (A) Patterning, electroplating, and CMP of counter electrodes and anchor post. (B) Patterning, electroplating, and CMP of the spring layer. (C) Patterning, electroplating, and CMP of the mirror support post and of the mirror layer. (D) Released continuous facesheet mirror attached to actuators [6].

Dr. Kubby and Dr. Fernandez have also designed and simulated different shapes of actuators using L-edit and finite element analysis (FEA) software in order to find the optimal spring support that would prevent tilting. The first design was a square actuator supported by eight folded springs at the corners as shown in figure (1.6a). The simulations of this design showed that it is capable of a displacement of approximately 9.8μm at 156 V, however, if there were any manufacturing asymmetries, the stiffness of the springs would not be uniform. This would cause the mirror to tilt and eventual premature pull in. The second design was a circular actuator supported by folded springs at 90,180,270 and 360 degrees around its perimeter as shown in figure (1.6b). This design was also able to achieve a displacement of approximately 9.9μm at 167 V. However, simulations showed that the perimeter of the circular actuator was not displaced less than the center. In addition, this actuator required a larger voltage compared to the square actuator. The last design was an X-beam actuator, which is basically a square actuator supported diagonally at the corners by fixed-fixed beams as shown in figure (1.6c). This design achieved approximately 10μm at a voltage of 280 V. The X-beam actuator minimized the tilting effect but required a large voltage compared to the previous designs discussed above. Since it is important that the center of the actuators be displaced more than the corners to prevent tilting, the X-beam actuator design was chosen. The X-beam has proven to provide the best spring support. Figure (1.7) represents the three designs after fabrication whereas figure (1.8) represents the fabricated three designs [5].

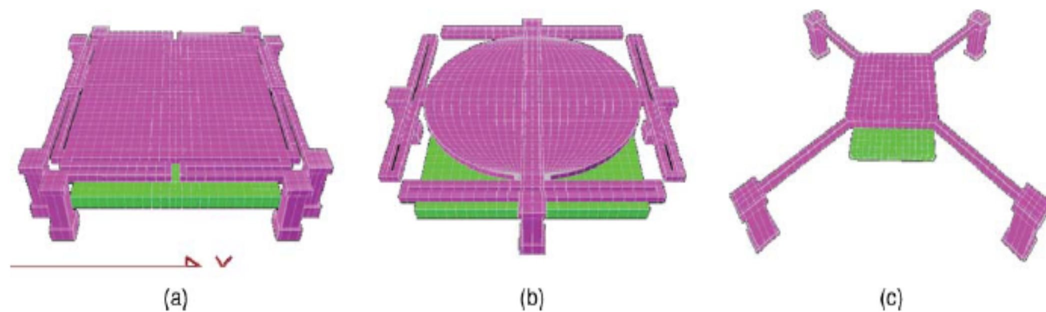

Figure 1.6: 3D actuator designs modeled with FEA. (A) Square actuators supported by eight folded springs at the corners. (B) Circular actuators supported by four folded springs. (C) X-beam actuators supported by four fixed-guided beams [5].

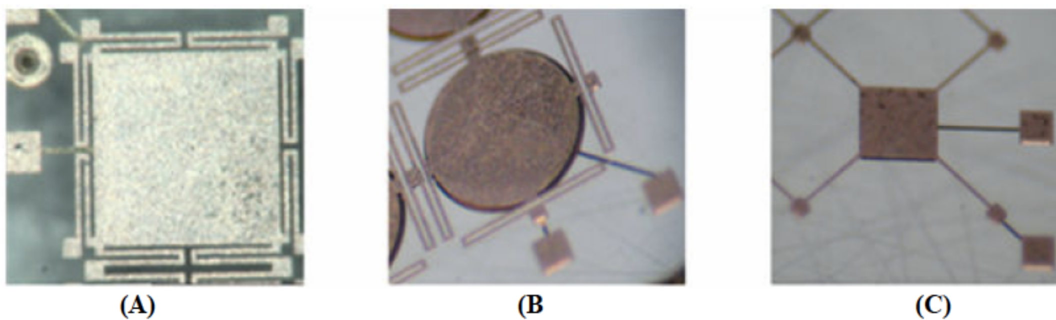

Figure 1.7: The three actuator's designs shown in Figure 1.6 fabricated out of gold [5].

1.4 X-Beam Actuator Design

The X-beam actuators were designed to prevent premature pull-in while achieving large displacement. The center square electrode in the x-beam actuator measures 400 x 400µm with four 390 x 20µm fixed-guided beams as shown in figure (1.6c). The actuator's fixed-guided beams become nonlinear when displaced by more than half of the spring layer thickness. This nonlinearity allows for mechanical strain or stiffening to increase the actuators travel range to more than half the gap [7]. Therefore, the actuator's spring can be described by a nonlinear spring equation as follows:

$$F_m = K \cdot z + K_s \cdot z^3 \qquad (1.9)$$

And the pull-in voltage becomes:

$$V_{pi} = \sqrt{\frac{2 \cdot \left(K \cdot z + K_s \cdot z^3\right) \cdot \left(g_0 - z\right)^2}{\varepsilon \cdot A}} \qquad (1.10)$$

Where K is the linear spring constant and K_S is the nonlinear stretching component. The linear MEMS spring constant is calculated by assuming that the actuator's beams are two parallel fixed-fixed beams as shown in figure (1.8):

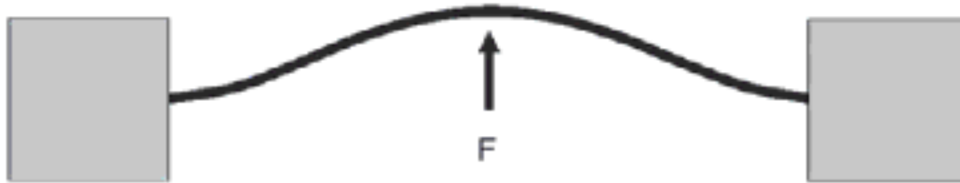

Figure 1.8: Fixed-fixed beam subjected to a point load F at the middle of the beam [3].

This spring constant is a function of Young's Modulus (E), the length of the spring's beam (L) and the moment of inertia (I) as given by the following equation:

$$K = \frac{384 \cdot E \cdot I}{L^3} \tag{1.11}$$

Since the moment of inertia is given by

$$I = \frac{w \cdot t^3}{12} \tag{1.12}$$

Where w and t are the width and thickness of the spring beams, respectively.

Therefore the spring constant K becomes:

$$K = \frac{384 \cdot E}{L^3} \cdot \frac{w \cdot t^3}{12}$$

$$K = \frac{32 \cdot E \cdot w \cdot t^3}{L^3} \tag{1.13}$$

Similarly, the nonlinear stretching component for a single fixed-fixed beam is given by the following equation:

$$K_s = \frac{\pi^4 \cdot E \cdot w \cdot t}{8 \cdot L^2}$$

And for two fixed-fixed beams the equation becomes:

$$K_s = \frac{\pi^4 \cdot E \cdot w \cdot t}{4 \cdot L^2} \qquad (1.14)$$

Therefore the mechanical force becomes:

$$F_m = \frac{32 \cdot E \cdot w \cdot t^3}{L^3} \cdot z + \frac{\pi^4 \cdot E \cdot w \cdot t}{4 \cdot L^2} \cdot z^3 \qquad (1.15)$$

The deformable mirrors discussed in this thesis consist of 16 x 16 array of actuators with a continuous facesheet as shown in figure (1.9). The inner 14 x 14 actuators can be tested individually from each other as well as in groups for multi-actuator testing. Each electrode in each actuator is routed and connected to a bond pad [6].

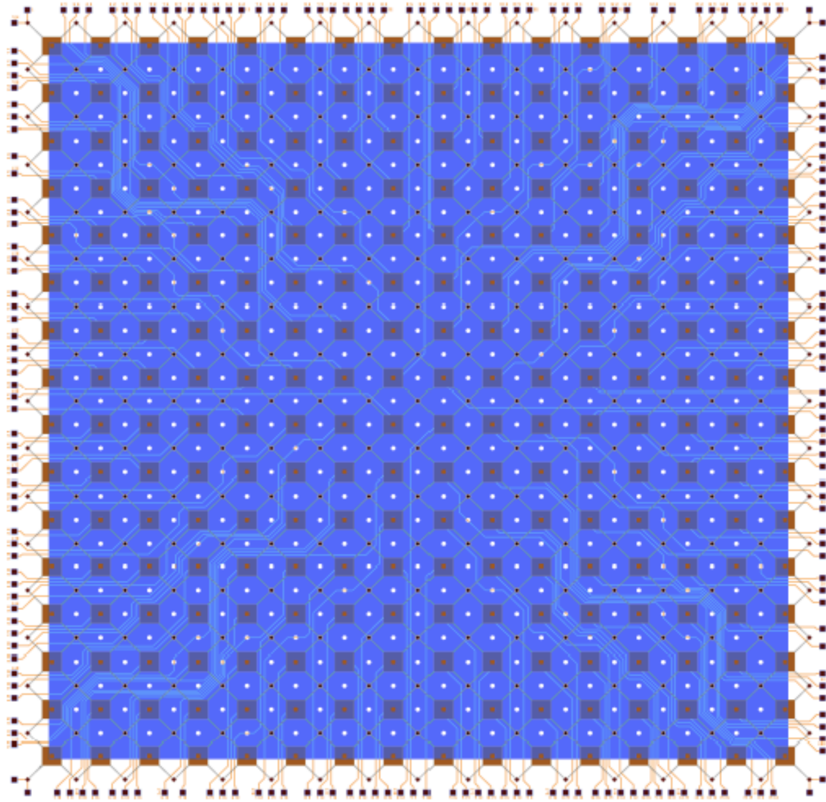

Figure 1.9: layout of 16x16 deformable mirror array [6]

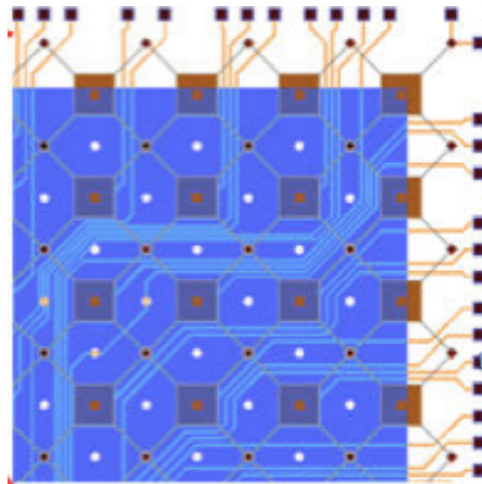

Figure 1.10: Close-up view of the top right of a 16x16 deformable mirror array [6]

Chapter 2: Deformable Mirror Testing

2.1 Actuator Packaging and PCB Test Board

The 16 x 16 actuator deformable mirrors were packaged onto a 181 gold-plated through-hole ceramic pin grid array (CPGA) as shown in figure (2.1). In order to actuate the largest number of actuators in a square area, the center 12 x 12 actuators were wire-bonded to the CPGA where the outer 2 rows of the deformable mirror are used as spring support for the continuous facesheet. In addition, these deformable mirrors were not hermetically sealed. A glass lid was taped to protect the mirrors from dust [6].

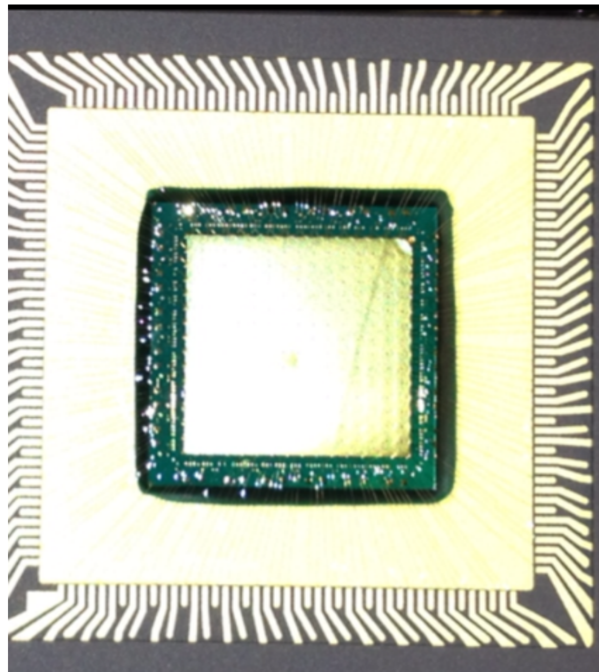

Figure 2.1: Packaged Deformable Mirror

The center 4 × 4 actuators of DMs were utilized for multi-actuator displacement testing. In order to perform the DM testing, a PCB was designed and fabricated as shown in figure (2.2). The PCB consists of two layers: the top layer, where the yellow traces are located and the bottom layer where the red traces are located. Also, the PCB has a ground plane (blue layer) at the bottom layer to help reduce noise. The PCB allows the actuation of 1 to 16 actuators with a single power supply by shorting a pin attached to a trace leading to the actuator of interest and a power pin. The deformable mirrors continuous facesheet is attached to the power supplies' ground. The packaged deformable mirrors were placed on a zero insertion force (ZIF) PGA test and burn-in socket (181-PRS 18041-12, Aries Electronics, Inc, Bristol, Pennsylvania) allowing the DMs to be easily swapped for testing. Table (2.1) gives the Die pad name (location of the actuator in the mirror layout), Die pad number and the equivalent package pad number of the center 4 x 4 actuators. Figure (2.3) shows the location of the actuators on the ZIF sockets, and figure (2.4) is an image of the ZIF socket mounted on the fabricated PCB.

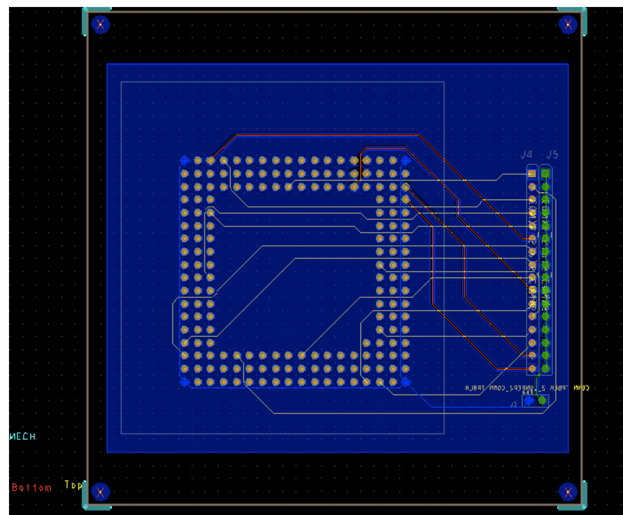

Figure 2.2: PCB layout for 16x16 deformable mirror

(7,7) 203 3	(8,7) 10 172	(9,7) 48 140	(10,7) 50 138
(7,8) 201 5	(8,8) 27 157	(9,8) 78 112	(10,8) 61 127
(7,9) 163 37	(8,9) 180 22	(9,9) 129 67	(10,9) 99 95
(7,10) 152 48	(8,10) 150 50	(9,10) 112 82	(10,10) 101 93

Table 2.1: The Die pad name, Die pad number and the equivalent package pad number of the center 4x4 actuators

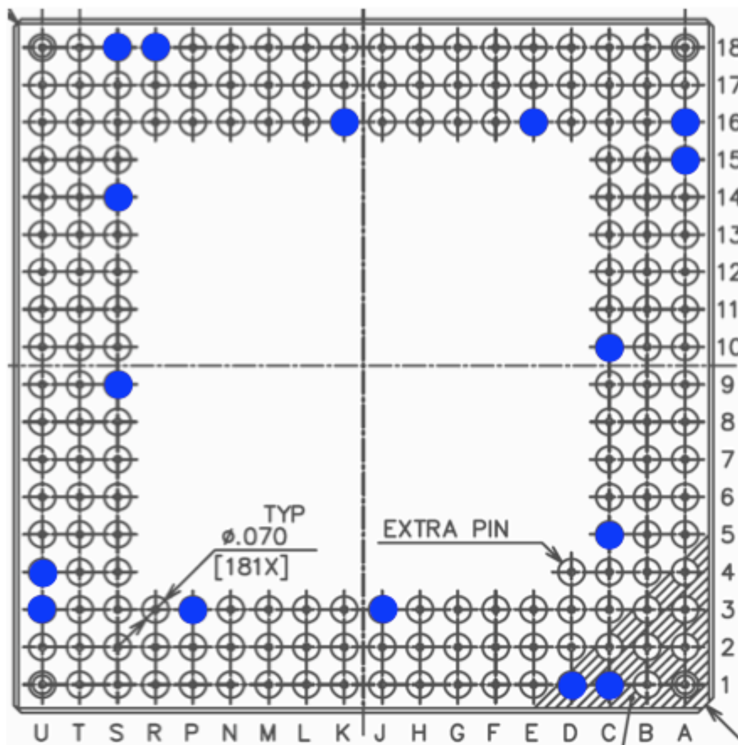

Figure 2.3: Location of the center 4x4 Actuator of the deformable mirror in the ZIF Socket

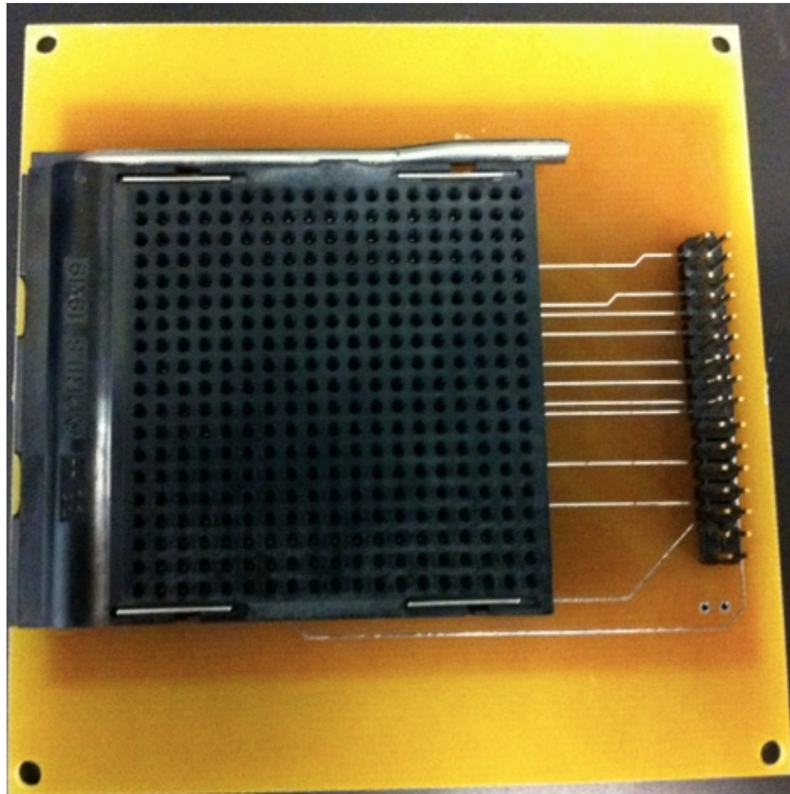

Figure 2.4: ZIF Socket Mounted on the fabricated PCB

2.2 WYKO Interferometer:

The Veeco WYKO ® NT1100 interferometer is used to test the deformable mirrors. This interferometer is an optical profiler providing accurate three-dimensional measurement of the surface topography of systems, ranging from a crystal surface to a MEMS deformable mirror. In this interferometer, the light reflects off of a reference mirror and combines with light from a sample to produce interference fringes. These fringes are alternating bright and dark bands of light. At the point of best contrast, we are able to obtain the best focus. The interferometer is able to take measurements via optical Phase-Shifting (PSI) and white light Vertical Scanning (VSI) and then outputs the scans and data to the WYKO Vision Software for analysis. In the testing of the deformable mirrors, the VSI mode is used. In this mode the white-light source is filtered with a neutral density filter, which preserves the short coherence length of the white light, and the system measures the degree of fringe modulation, or coherence, instead of the phase of the interference fringes [8]. Figure (2.5) represents the flow chart of the VSI algorithm used to extract the interference signal. Figure (2.6) gives a schematic of the interferometer. And figure (2.7) is an image of the WYKO interferometer.

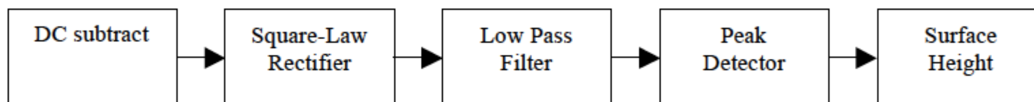

Figure 2.5: represents the flow chart of the VSI algorithm used to extract the interference signal [8]

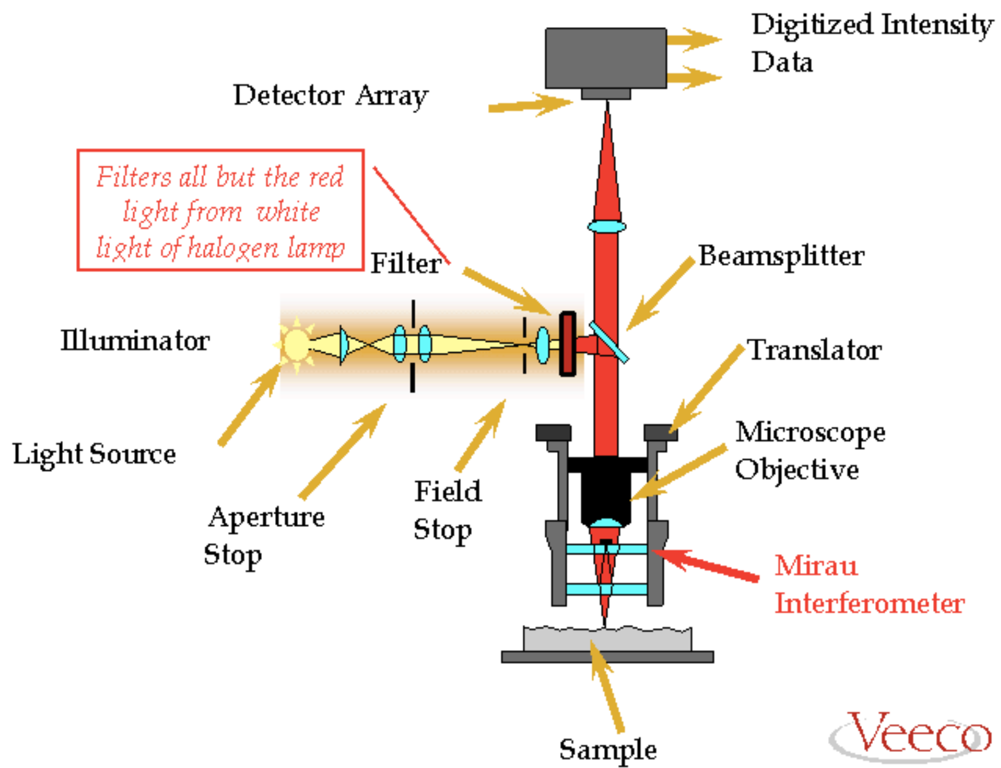

Figure 2.6: Schematic representation of the Veeco WYKO interferometer

Figure 2.7: Image of the WYKO interferometer used for testing the deformable mirrors

2.3 Testing Procedure

The following procedure describes how to set up the Veeco vision software and apply voltage to actuate the deformable mirror using the WYKO interferometer:

1) Connect the power supply probes so that the ground probe is connected to the ground bond pad and the voltage probe connected to the desired actuator's bond pad.
2) Click on measurement options to set measurement type to VSI, Objective to 2X and the field of view (FOV) to 0.5X.
3) Under the same window click on VSI options to set the Backscan that is the distance the camera will vertically move upwards to take measurements. Set the length that is the downward distance measured. And the threshold modulation, which is the percentage ratio where the higher the percentage the higher the accuracy. The appropriate values for testing the deformable mirrors discussed in this thesis are as follows:

   Backscan: 10 μm
   Length: 80 μm
   Modulation Threshold: 1%

4) Fluff the fringes at the bottom layer and then bring them back to the top layer. Align the fringes with the desired actuator as shown in figure (2.8)

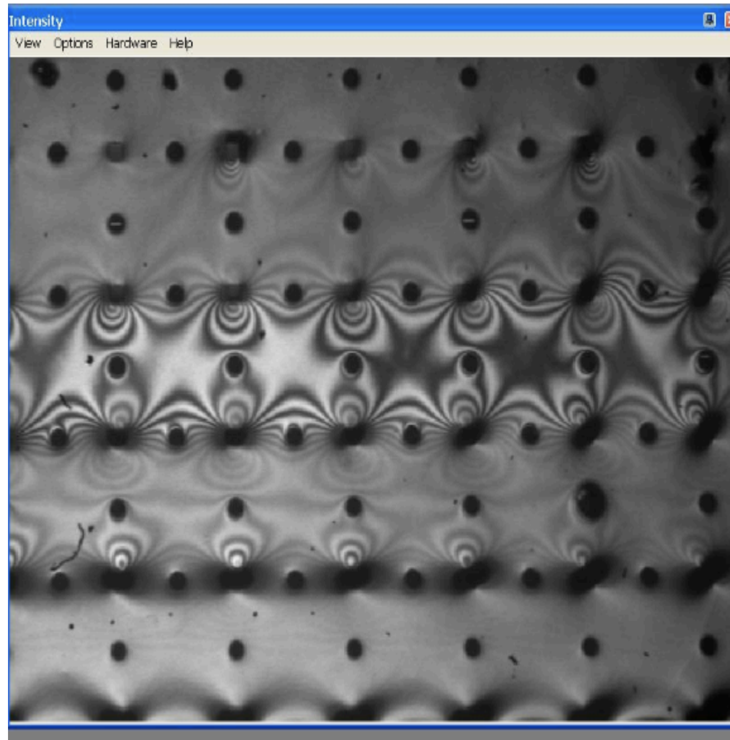

Figure 2.8: Fringes of the deformable mirror

5) Take a scan and then go to the Mask Editor option. Choose histogram and drag the cursors to frame the wavelengths of about 500 nm. Next choose the mask type "right " or "left" which will remove the values in the histogram of that type and then click ok. The software will try to align the device by referencing the wavelength chosen in the histogram as shown in figure (2.9) and figure (2.10). Next, click on terms, save then ok.

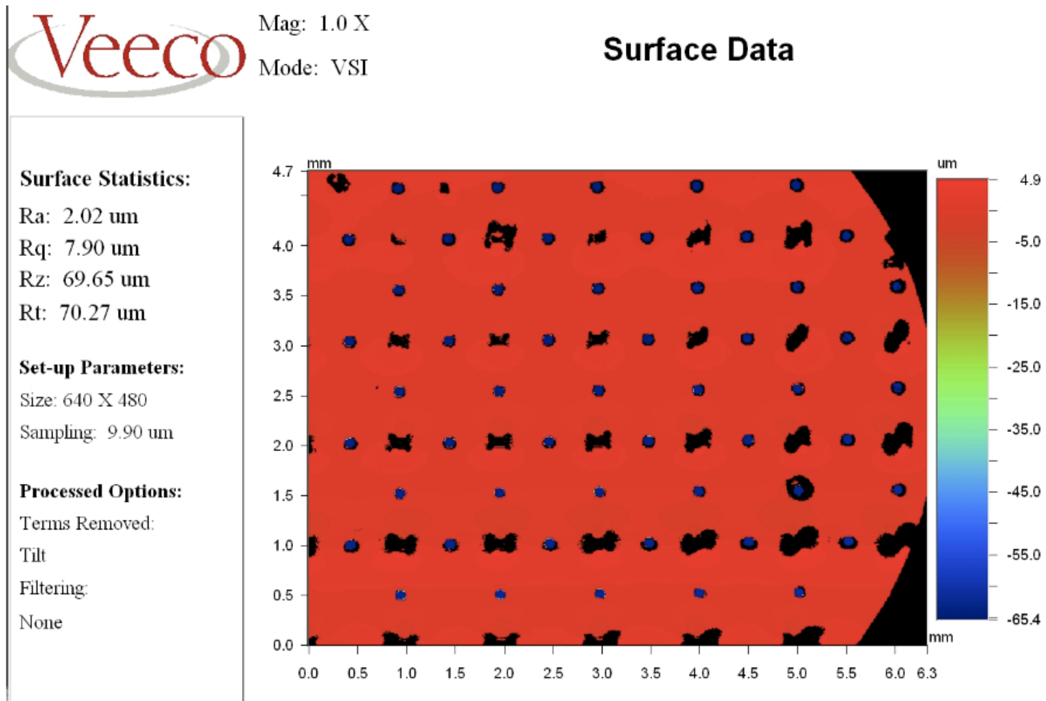

Figure 2.9: Surface Scan of a deformable mirror before alignment

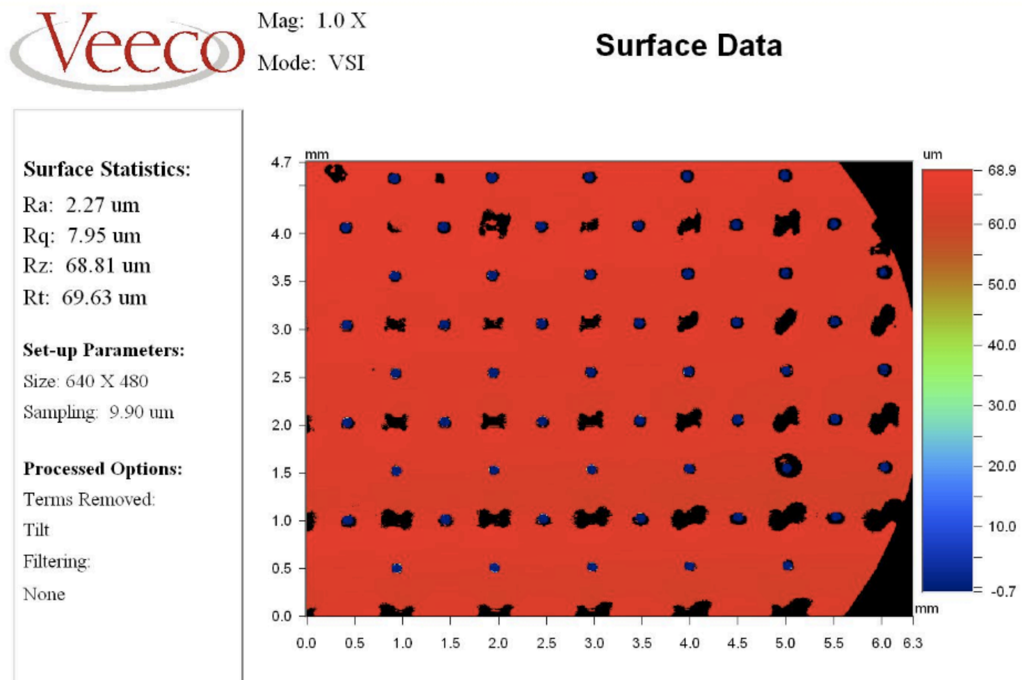

Figure 2.10: Surface Scan of a deformable mirror after alignment

6) Next click on SV option tab and create a new template. Click on raw data and set the maximum slope to between 10 -20 degrees and the minimum island between 5 – 10 pix as shown in figure (2.11). Click next and pick two islands.

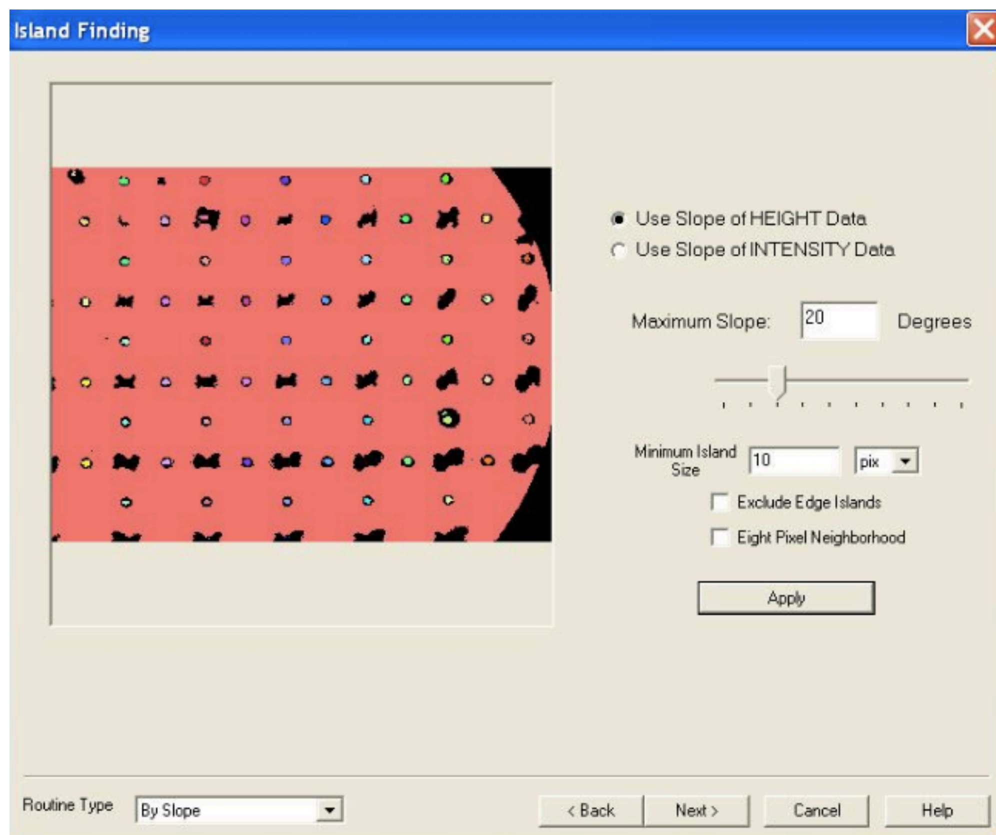

Figure 2.11: Window for setting the maximum slope and minimum islands

7) Click next and define the actuators of interest by drawing squares around them. After pick all etch hole as a reference as shown in figure (2.12). The reference region is the feature of zero (remove tilt from). Parameters for the other regions are calculated relative to the reference region.

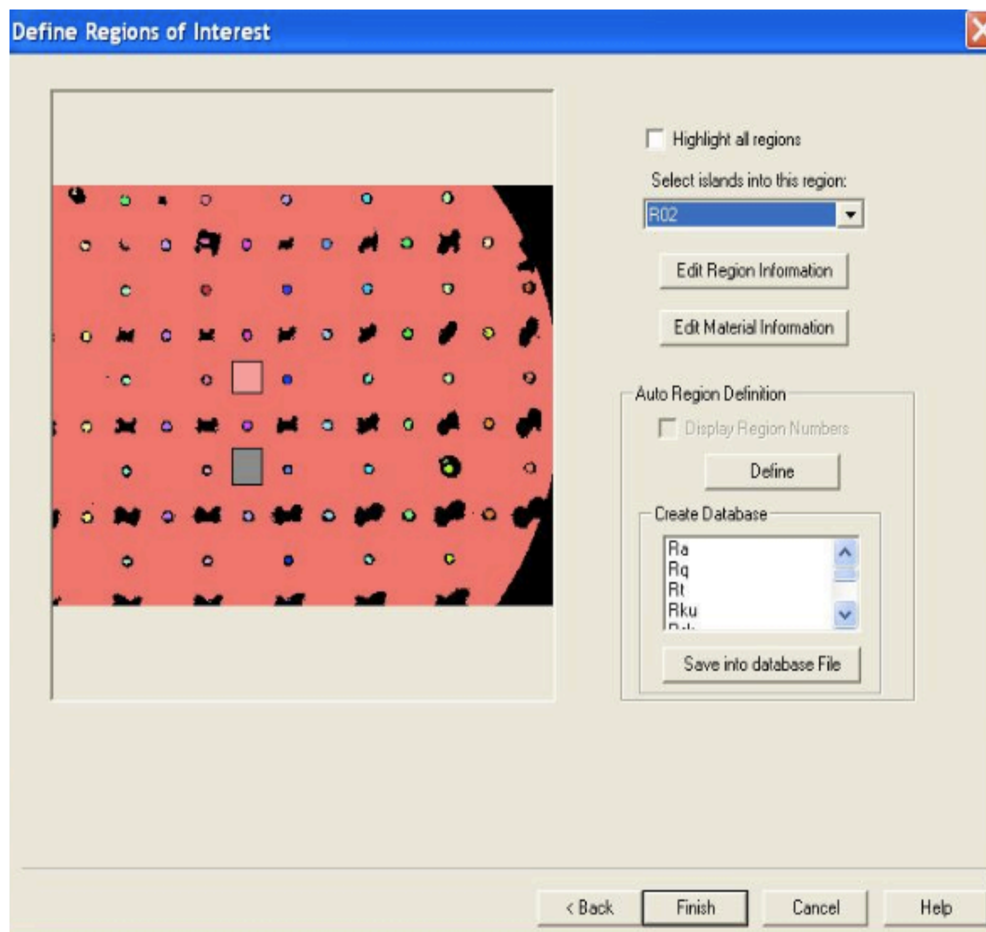

Figure 2.12: Window for defining the actuators of interests and references

8) After, select R01 through R09 depending on how many actuators are going to be tested. In figure (20) two actuators are tested, therefore pick R01 for the top actuator and R02 for the bottom actuator.

9) After click finish and then calculate to get the screen shown in figure (2.13).

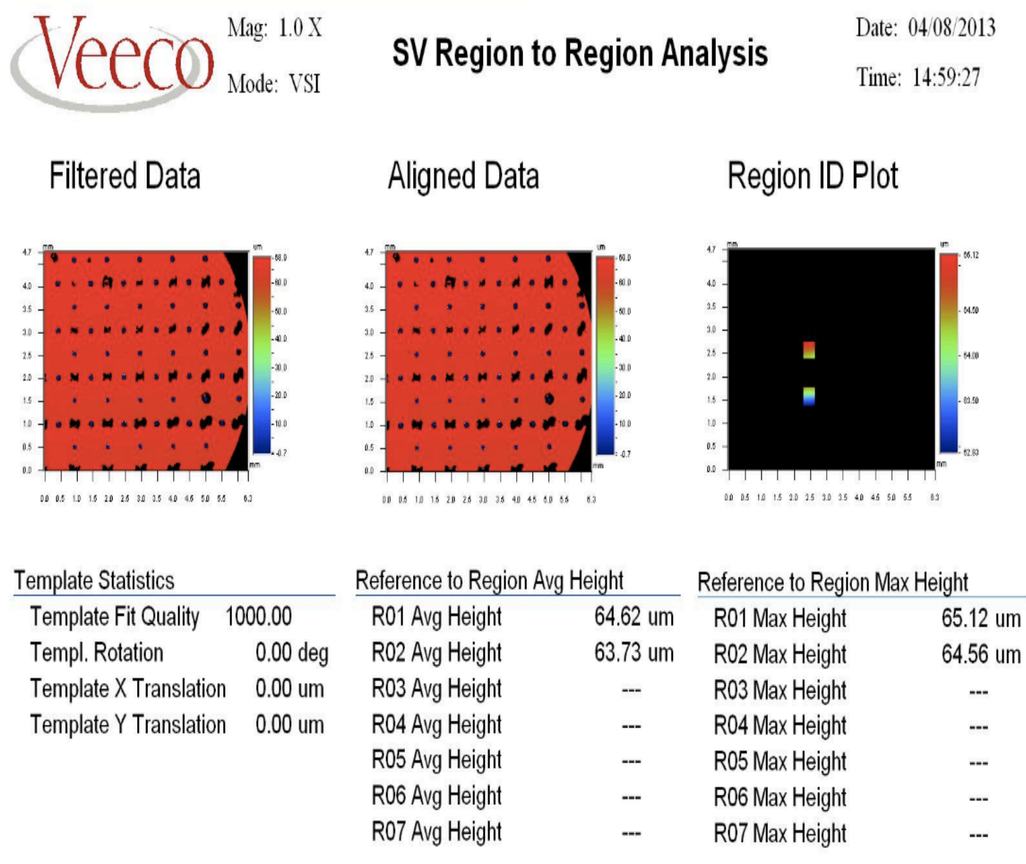

Figure 2.13: Window after finishing the set up and calculating the initial heights of the actuators of interest

10) After click on the database tab and choose database options and then define. Scroll down for SV analysis and add Average height for R01 through R09. Depends on how many actuators are been tested. In figure (2.12) they were two actuator that are been tested so pick

RO1 Avg Height ad then click ADD
RO2 Avg Height ad then click ADD

11) Once the average heights are added you can start applying voltage and scanning. In the database window, click View and choose graph to keep track of the behavior of your device as shown in figure (2.14).

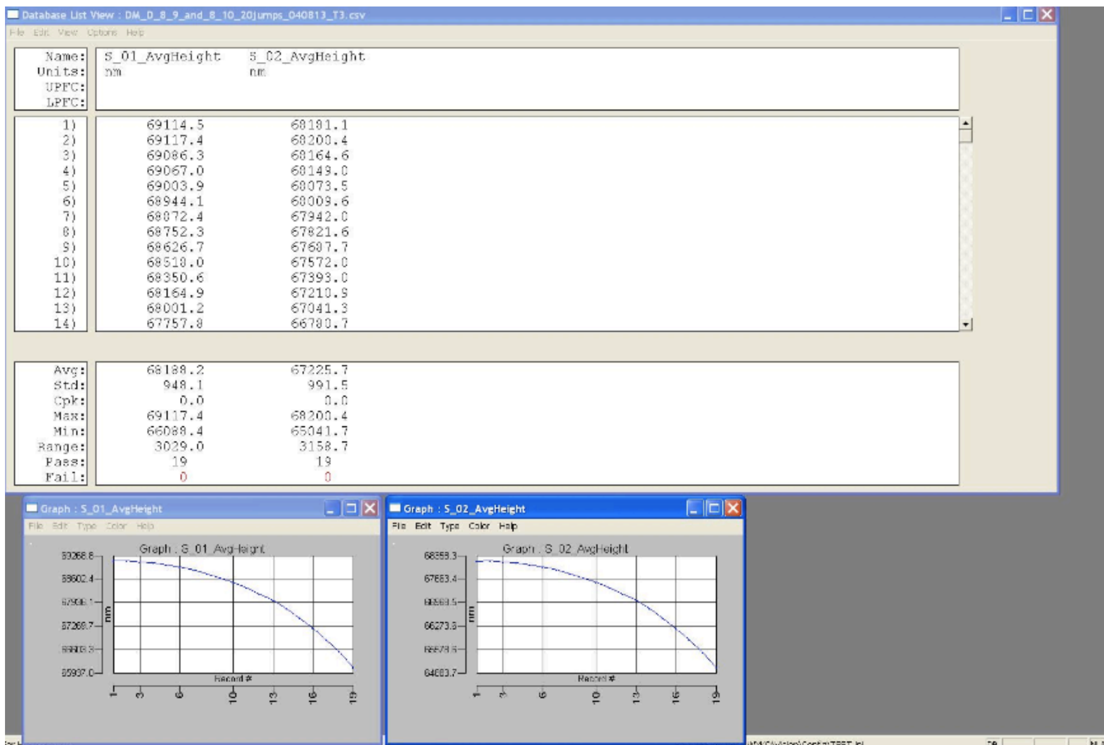

Figure 2.14: Database view and graphs of displacement vs. voltage for dual actuator testing.

Chapter 3: Deformable Mirror Testing Results

3.1 Challenges

Previously, single actuators of a 10×10 deformable mirror were tested and scanned using a white light interferometer. The center four actuators of this DM were actuated. The average displacement, due to an applied voltage of 300V, was found for each quadrant. The average displacement ranged from 2.62 to 6.26μm. And as expected, the more voltage applied the larger the displacement as shown in figure (3.1). This figure represents 5 trials of voltage vs. displacement for a single actuator in a 10 x 10 actuators deformable mirror [6].

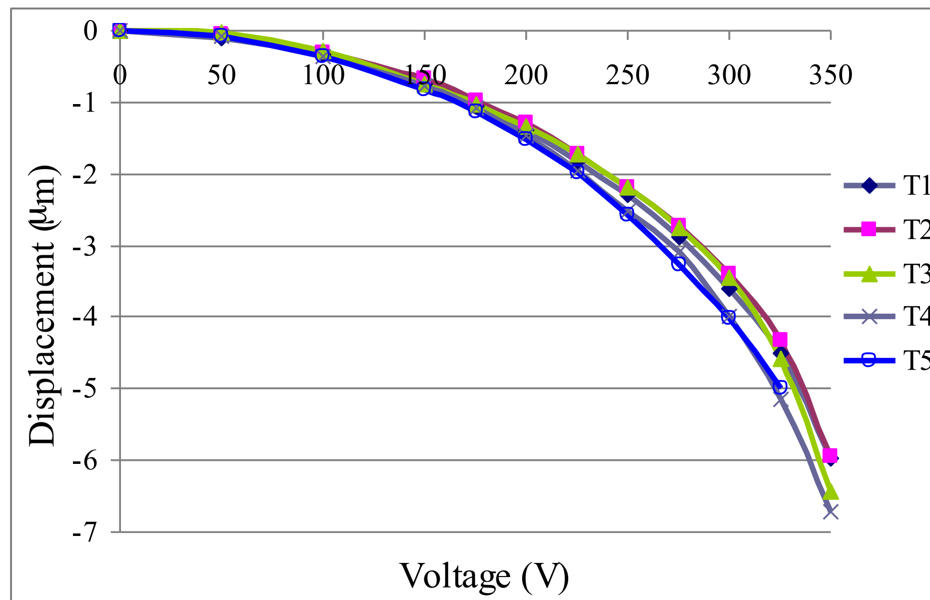

Figure 3.1: Displacement vs. voltage for a 10x10 mirror system [6].

From these obtained results we can assume that actuating multiple actuators in a 16x16 actuator deformable mirror from the same die should behave in this manner as shown in figure (3.1). However, the initial testing of the central 4x4 actuators exhibited different behavior. Initially, there was no movement on the center of the DM. The DM was scanned across using the interferometer and some movements were observed on some actuators. However, these actuators do not correspond to the actuators near the center as expected. These actuators are far apart from each other and cannot be used for multi-actuator actuation. The pins and pad numbers were doubled, checked with the designed PCB and everything matched according to table (2.1). In addition, pin 1 of this deformable mirror was found to be wire bonded to pin 46 and not pin 1 as was requested. Another issue encountered was that applying voltage to certain actuators showed oscillation in the displacement; they oscillated back and forth even as the voltage increased all way up to 320 V, as shown in figure (3.2). This result could possibly lead to the conclusion that this mirror may not be fully released and/or the fact that there might be a humidity factor responsible for this behavior

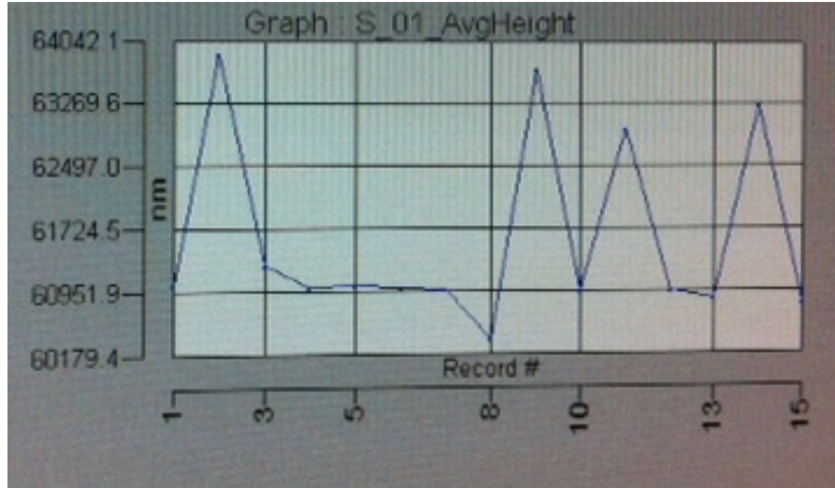

Figure 3.2: Oscillating behavior in the Displacement vs. voltage graph for a dual actuator-system testing

Further testing of the mirrors suggested that there is a 90-degree rotation of the mirror packaging compared to what was expected. In order to confirm that there is indeed a 90-degree rotation, the wires from the mirror to the package were traced using a probe station shown in figure (3.3). It was found that this mirror's packaging is rotated 90 degrees counter-clockwise. After examining the rest of the mirrors (total of 6) it was found that two mirrors were rotated 90 degrees clockwise, two were rotated 90 degrees counter-clockwise, and the last two were correctly packaged. In addition, it seems like there is an additional horizontal flip as shown in figure (3.4) and (3.5). Figure (3.4) represents the pin array of the ZIF socket used for testing and figure (3.5) represents the DM packaging. The blue lines and dots are the center 4x4 actuators expected while the red lines and dots are the actuators obtained.

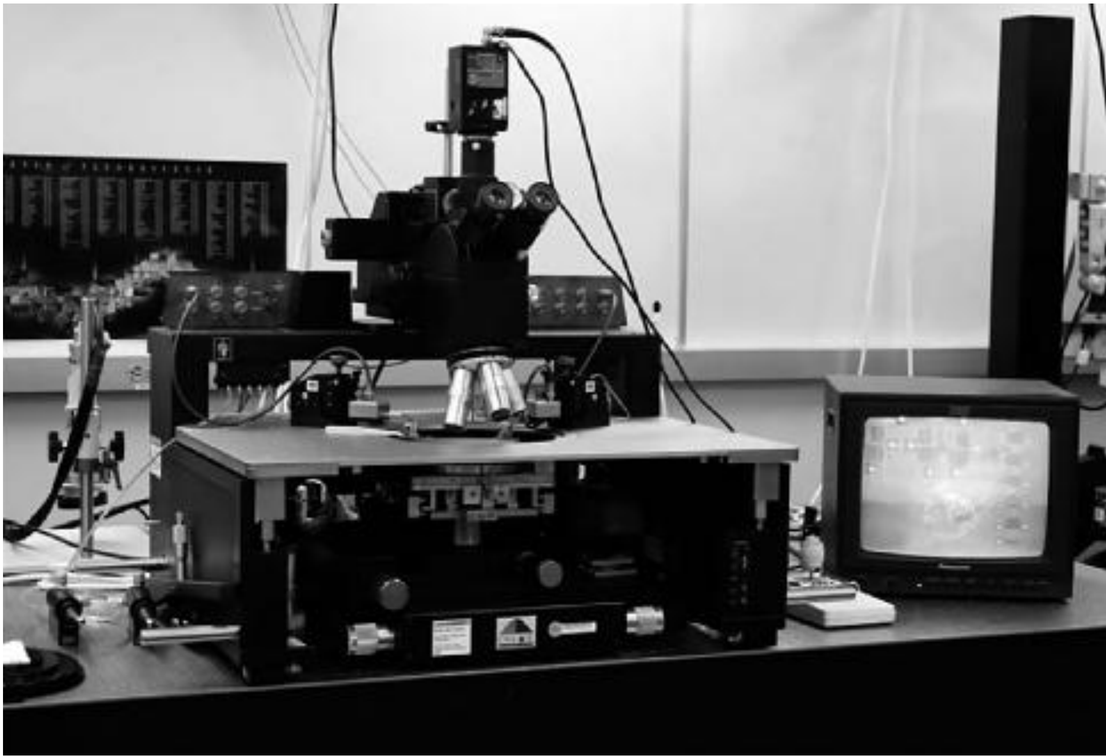

Figure 3.3: Probe station used for electrical and mechanical probing

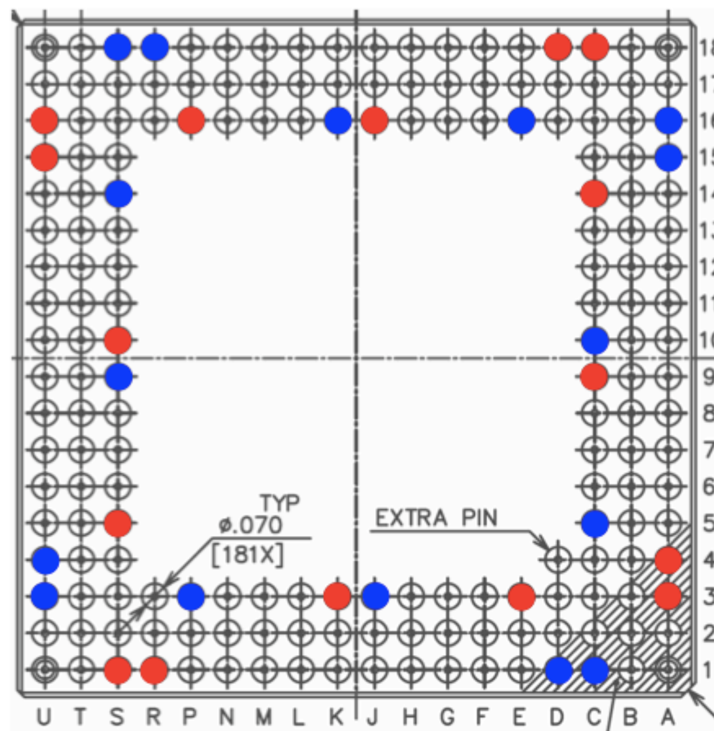

Figure 3.4: ZIF socket pin array. Blue dots represent the pins wanted. Red dots represent the pins obtained

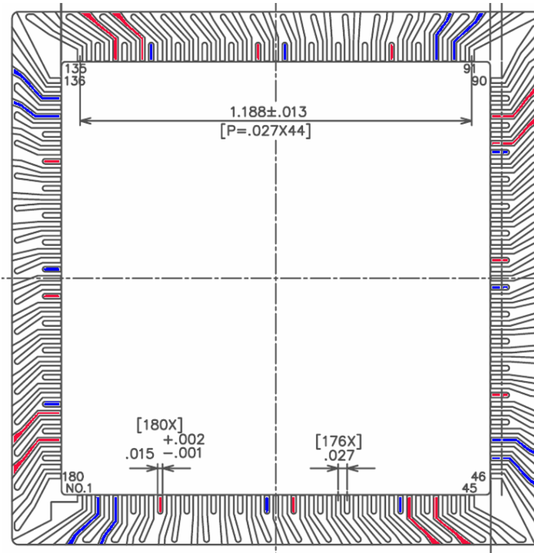

Figure 3.5: DM Packaging. Blue lines represent the pins wanted. Red lines represent the pins obtained

According to these results a new PCB was designed and sent for fabrication. The new PCB was horizontally flipped. It was also modified by adding keep out shapes around the voltage actuator connector and around the ground and voltage pin as shown in figure (3.6).

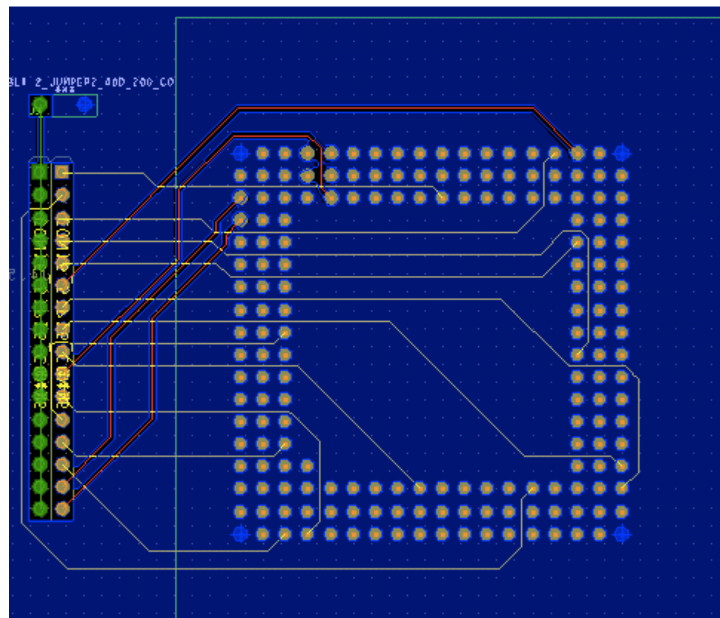

Figure 3.6: Layout of the Horizontally flipped PCB

Since the PCB was flipped horizontally, the mirrors will be simply rotated either CW or CCW and placed in the ZIF socket as shown in the following figures (3.7), (3.8) and (3.9).

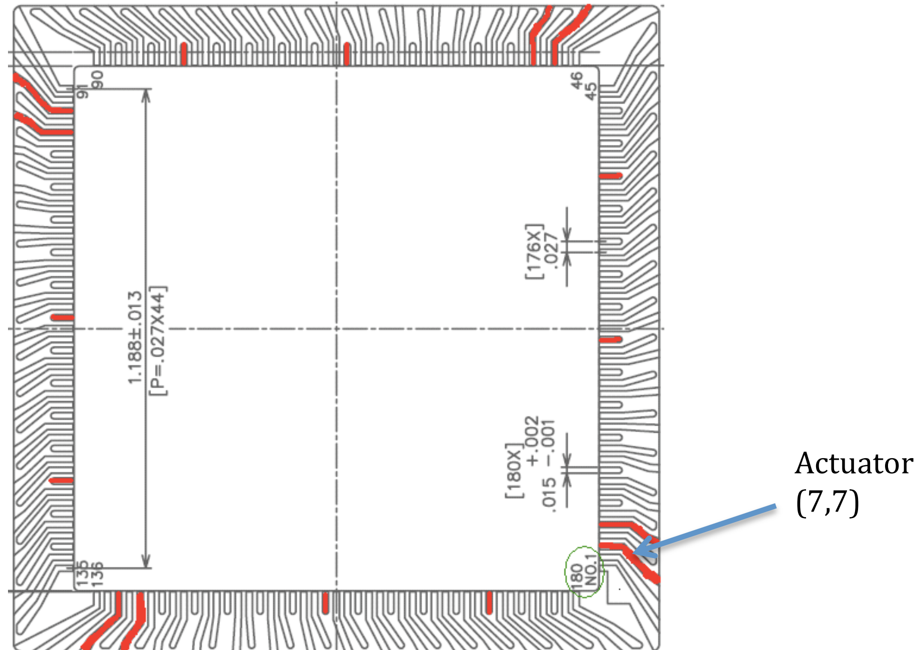

Figure 3.7: Correct orientation of the mirror with respect to packaging

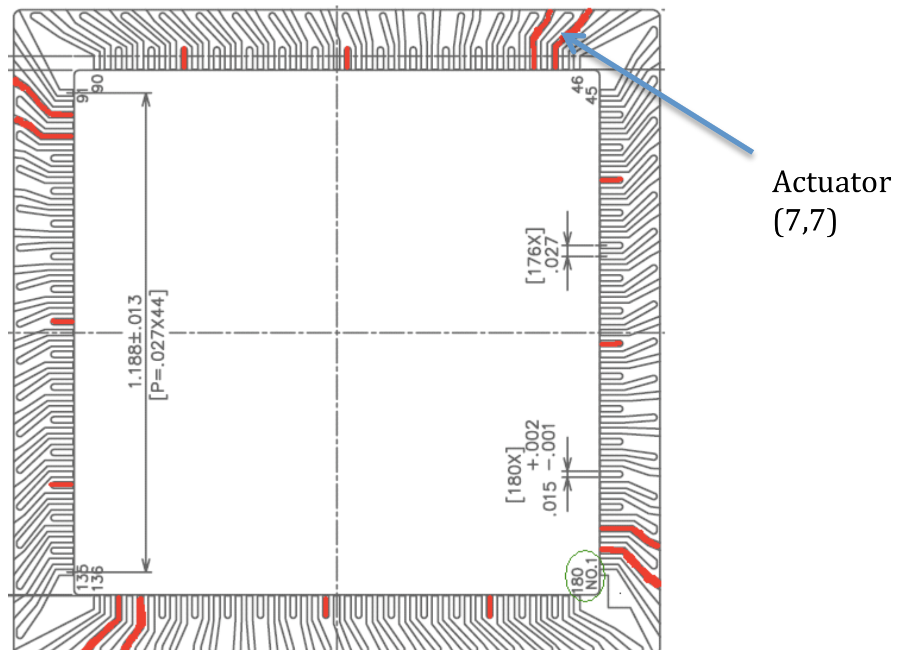

Figure 3.8: 90 degrees CCW orientation of the mirror with respect to packaging

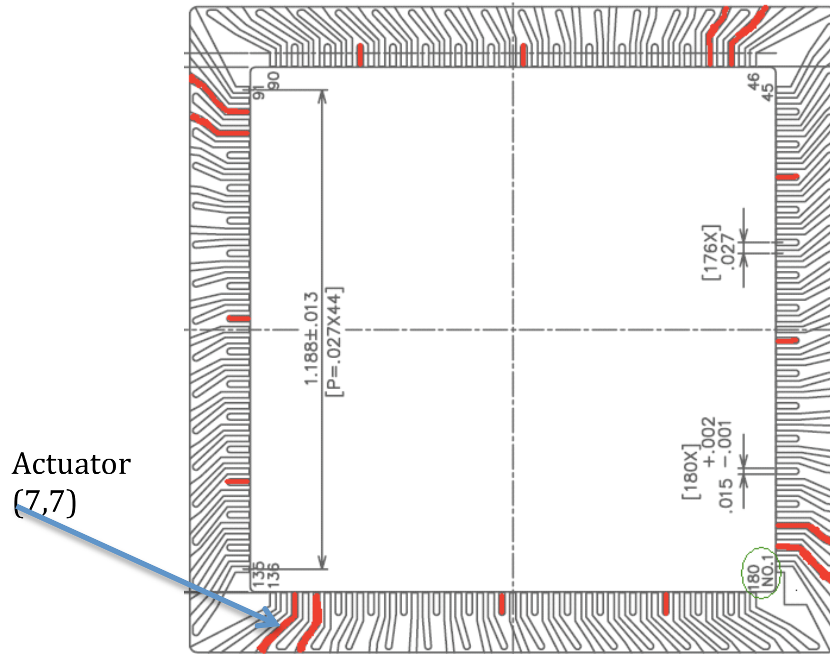

Figure 3.9: 90 degrees CW orientation of the mirror with respect to packaging

3.2 Results

Due to damage in the center of the deformable mirror, as shown in figure (3.10), during the fabrication process, only 4 actuators behaved as expected. In addition, some packaging wires got removed by mistake, which made the bottom two rows of actuators unavailable for testing. Only actuators (7,7), (7,8), (10,7) and (10,8) were individually tested. After, dual actuator testing was performed for actuators (7,7), (7,8) together and for (10,7) and (10,8) together.

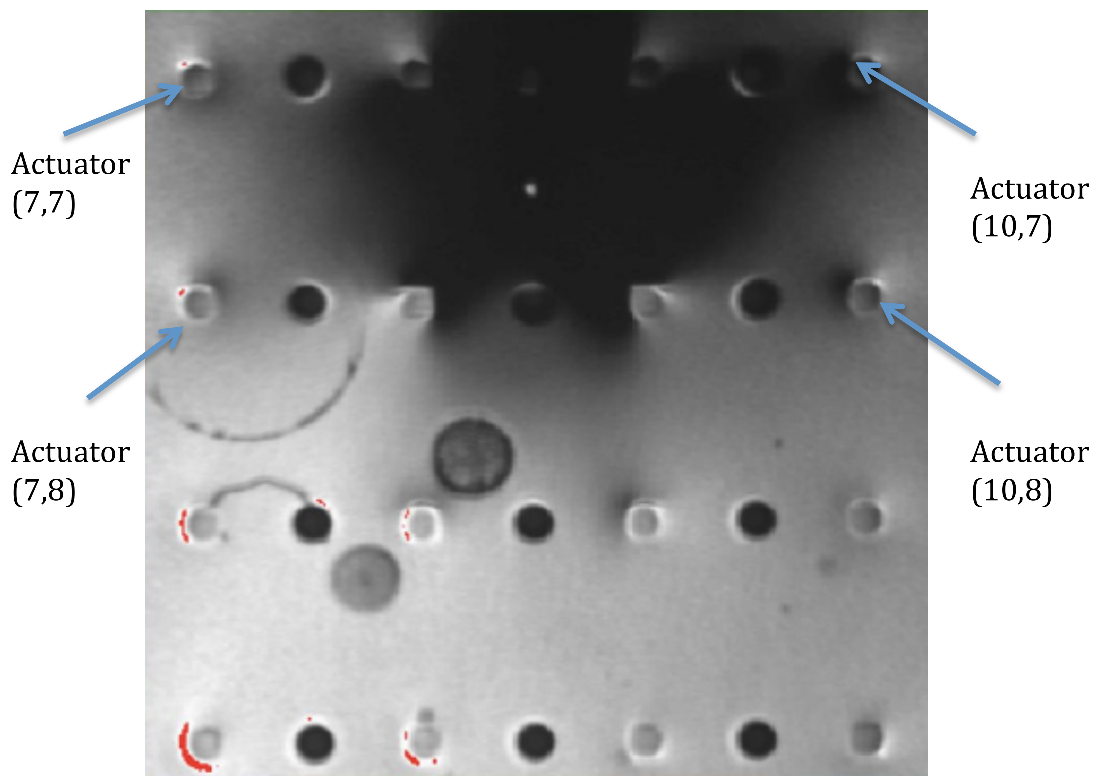

Figure 3.10: Center 4 x 4 actuators of the deformable mirror with the hole in the top

3.2.1 Individual Actuator Testing

Each actuator was tested individually and displacements were recorded for voltages from 0 - 360 V for actuator (7,7) and 0 - 380 V for actuator (10,7) and (10,8). Three trials of actuator (7,7) have been conducted leading to the graph on figure (3.11). While four trials of actuator (10,7) and (10,8) testing has been conducted leading to the two graphs on figures (3.12) and (3.13), respectively. These actuators follow the same trend that we expect; the more voltage you apply the more displacement in the z-direction. The maximum voltage applied results in an average displacement of 4.15 µm for actuator (7,7) at 360 V, 5.12µm for actuator (10,7) at 380 V and finally 4.58µm for actuator (10,8) at 380 V.

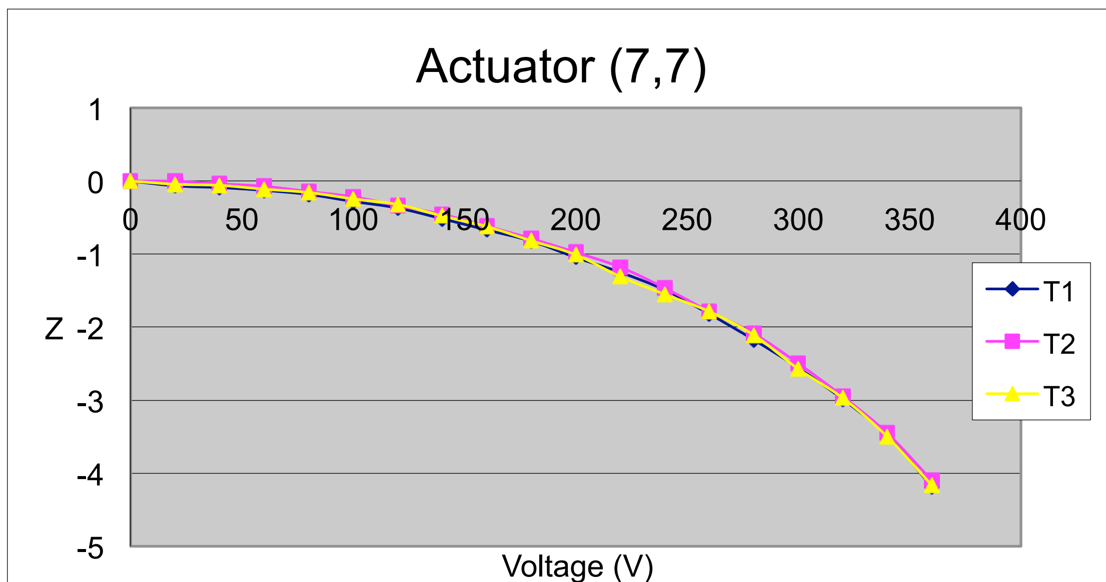

Figure 3.11: Graph of voltage vs. displacement for actuator (7,7)

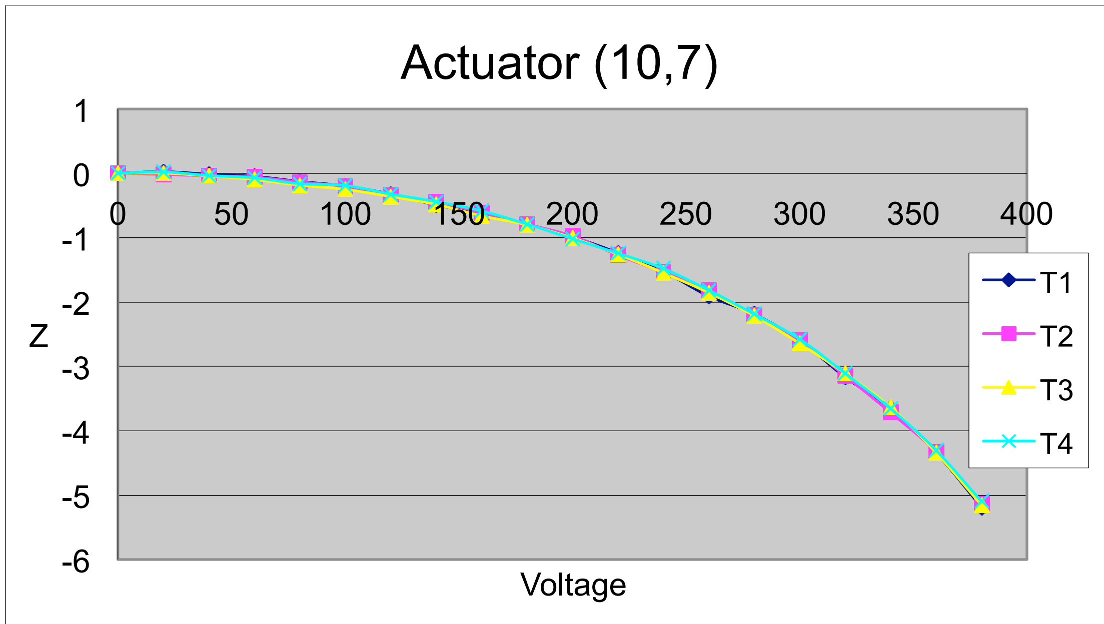

Figure 3.12: Graph of voltage vs. displacement for actuator (10,7)

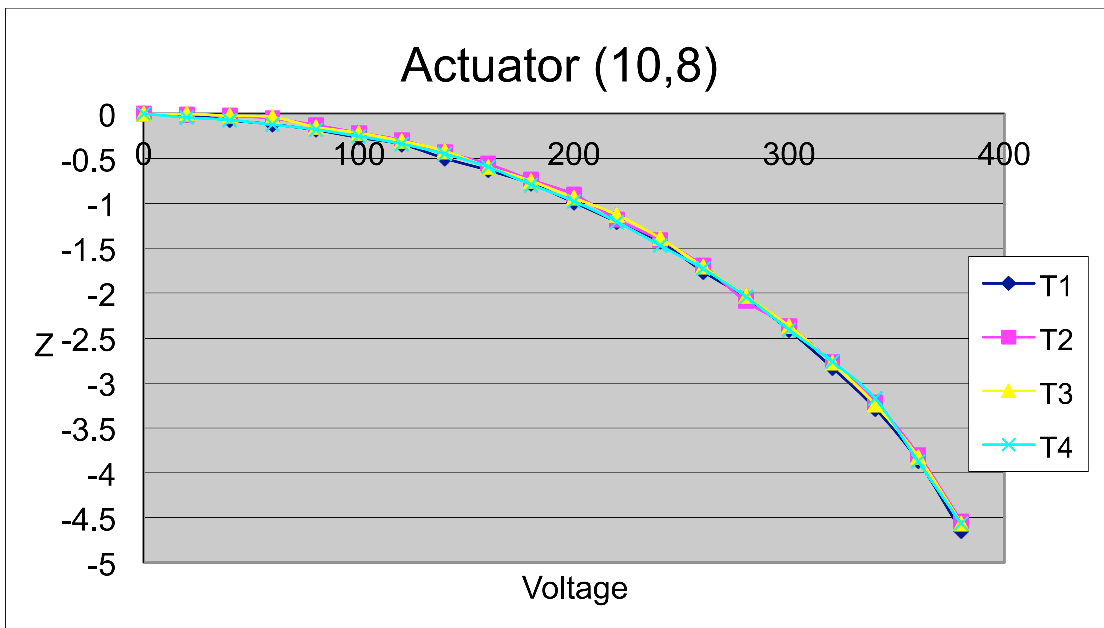

Figure 3.13: Graph of voltage vs. displacement for actuator (10, 8)

3.2.2 Two-Actuators Testing

The data below represents the displacements of two neighboring actuators, (7,7) and (7,8), being actuated at the same time under the same voltage. Three trials were conducted leading to the graphs in figures (3.14), (3.15) and (3.16). Both of these actuators follow the same trend that we expect; the more voltage you apply the more displacement in the z-direction. The maximum voltage applied to the dual actuation of (7,7) and (7,8) is 370 (V) leading approximately to a displacement of 7μm for actuator (7,7) and 6μm for actuator (7,8).

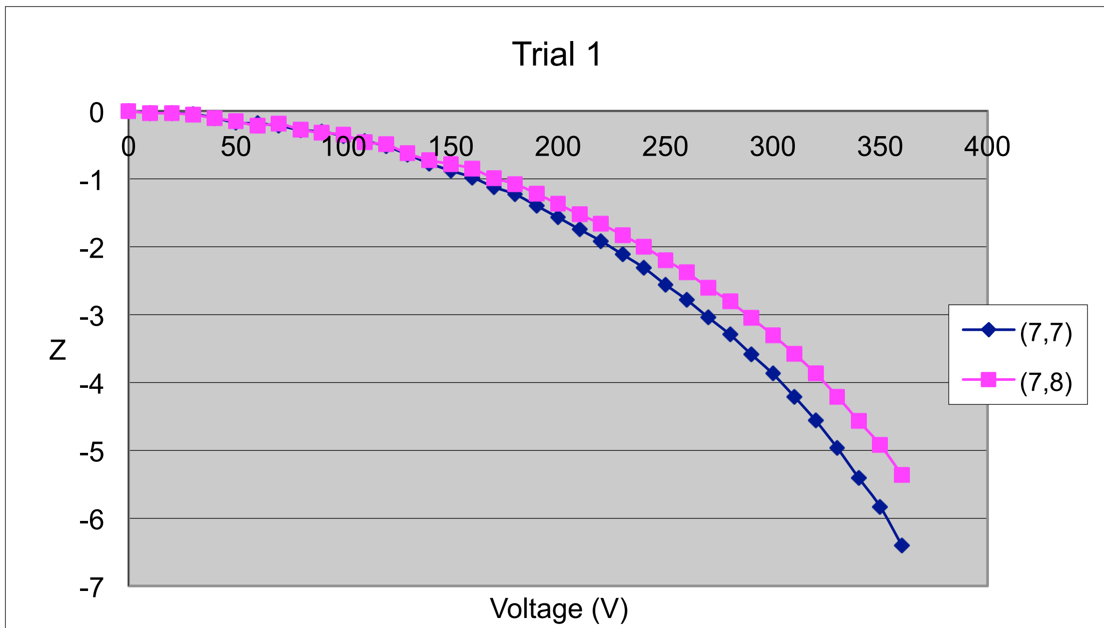

Figure 3.14: Trial 1 for dual actuator testing for actuator (7,7) and (7,8)

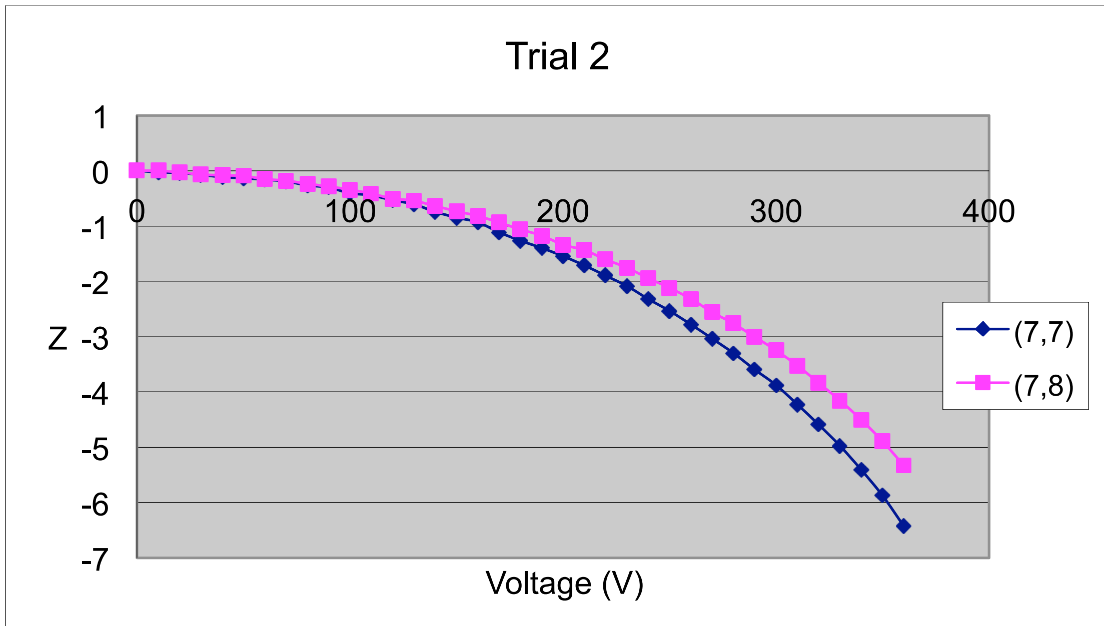

Figure 3.15: Trial 2 for dual actuator testing for actuator (7,7) and (7,8)

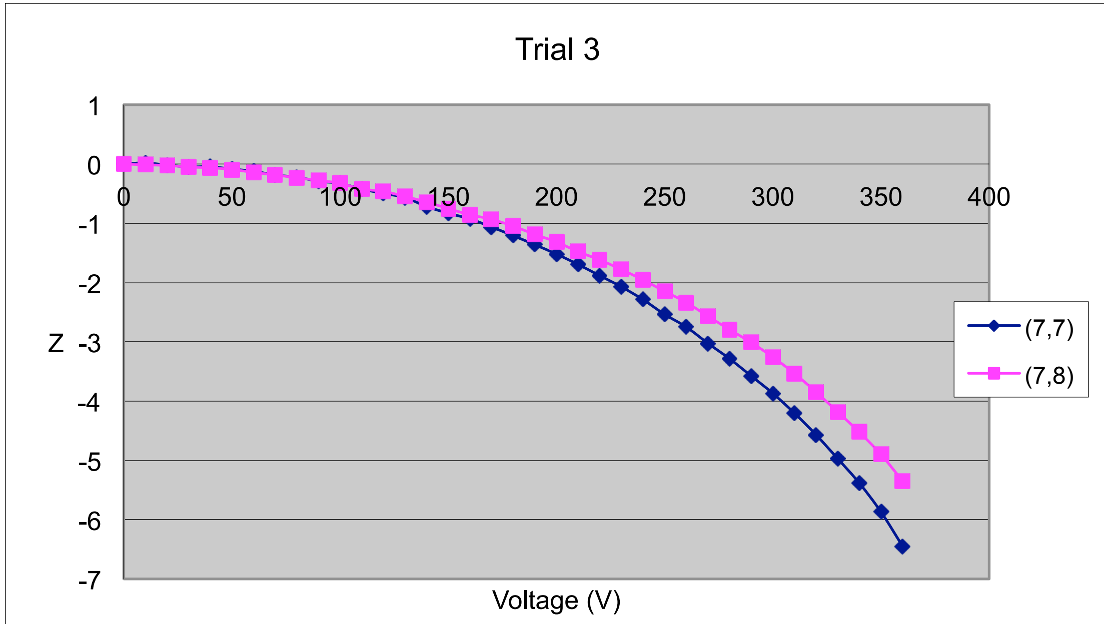

Figure 3.16: Trial 3 for dual actuator testing for actuator (7,7) and (7,8)

Similarly, four trials were conducted of the dual actuation of (10,7) and (10,8) leading to the graphs in figures (3.17), (3.18), (3.19) (3.20). The maximum voltage applied to the dual actuation of (10,7) and (10,8) is 380 V leading to an approximate displacement of 6.43μm for actuator (10,7) and 5.7μm for actuator (10,8). Once again, both of these actuators follow the same trend that we expect; the more voltage you apply the more displacement in the z-direction.

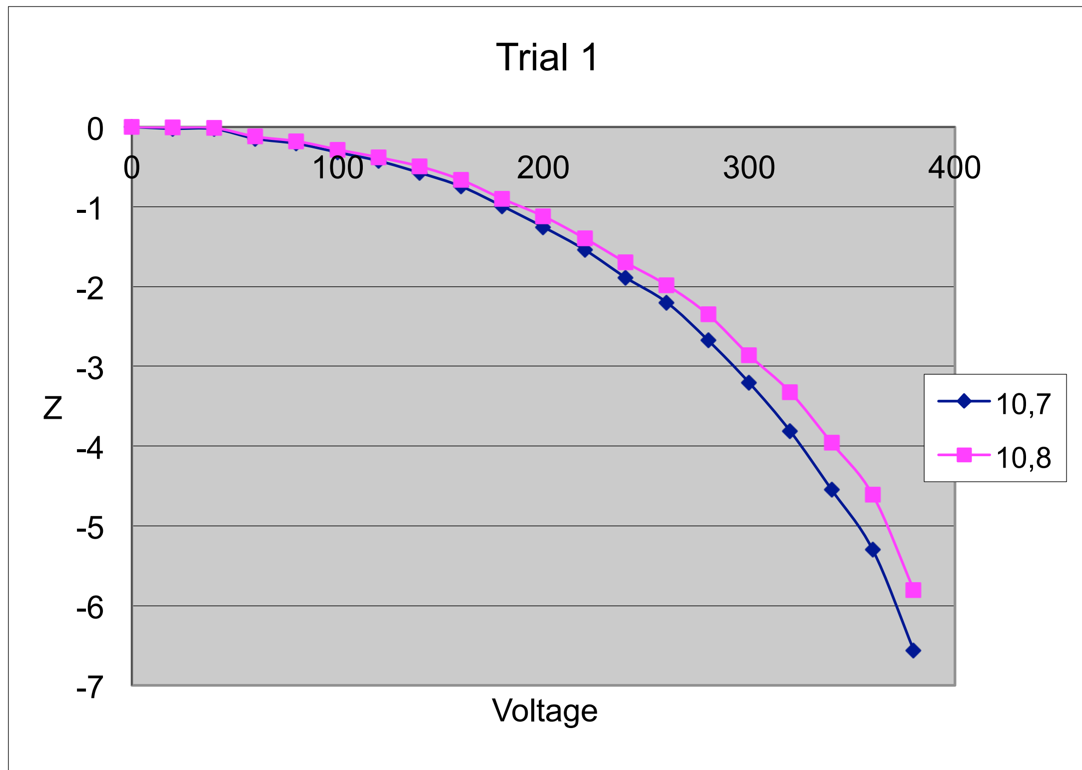

Figure 3.17: Trial 1 for dual actuator testing for actuator (10,7) and (10,8)

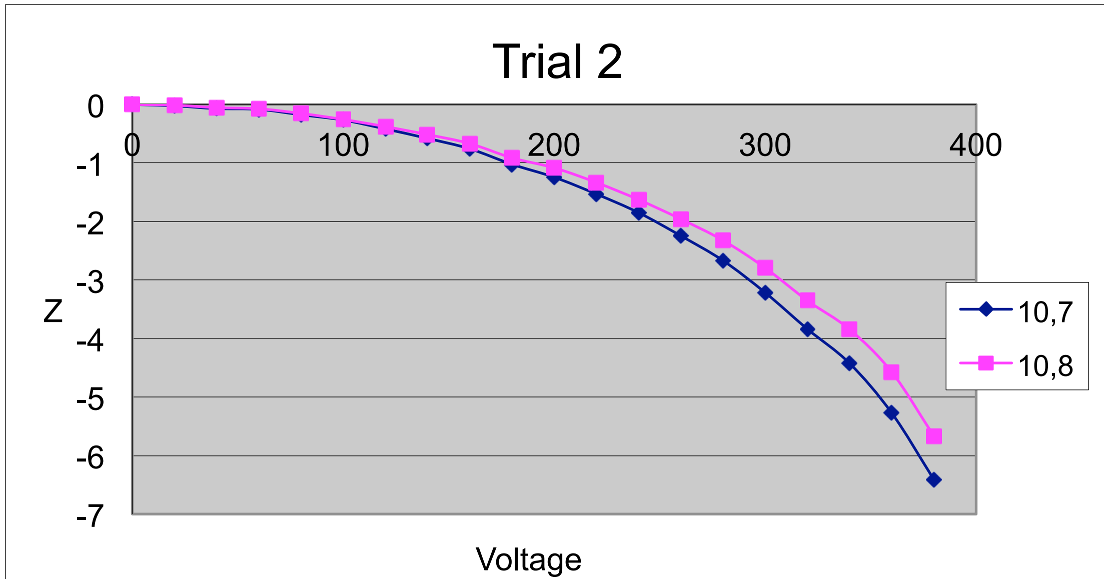

Figure 3.18: Trial 2 for dual actuator testing for actuator (10,7) and (10,8)

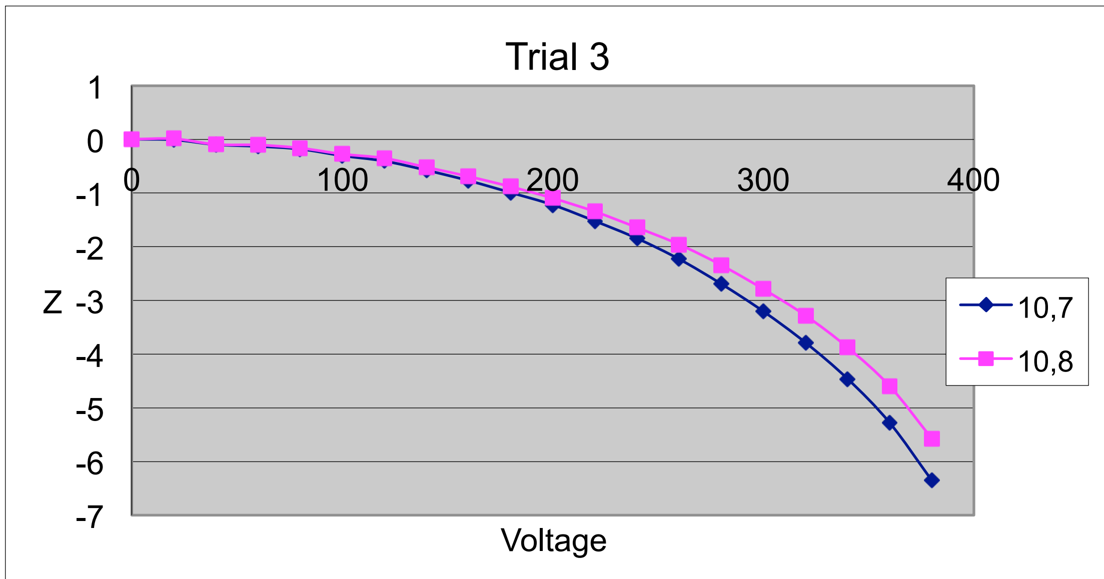

Figure 3.19: Trial 3 for dual actuator testing for actuator (10,7) and (10,8)

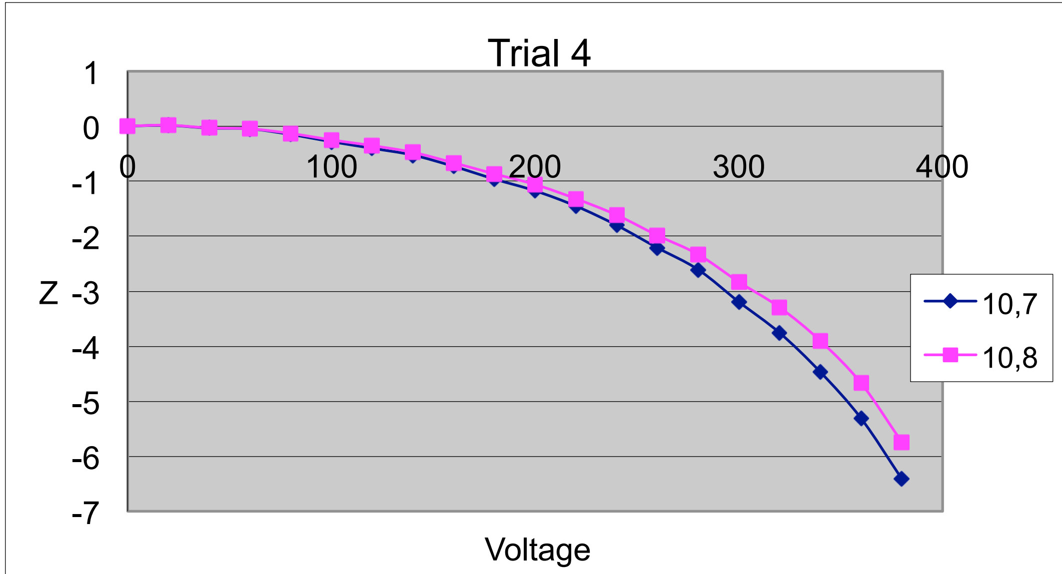

Figure 3.20: Trial 4 for dual actuator testing for actuator (10,7) and (10,8)

The graphs below in figures (3.21), (3.22), (3.23) and (3.24) show the repeatability of each actuator in dual testing leading to the conclusion that these actuators are indeed behaving as expected.

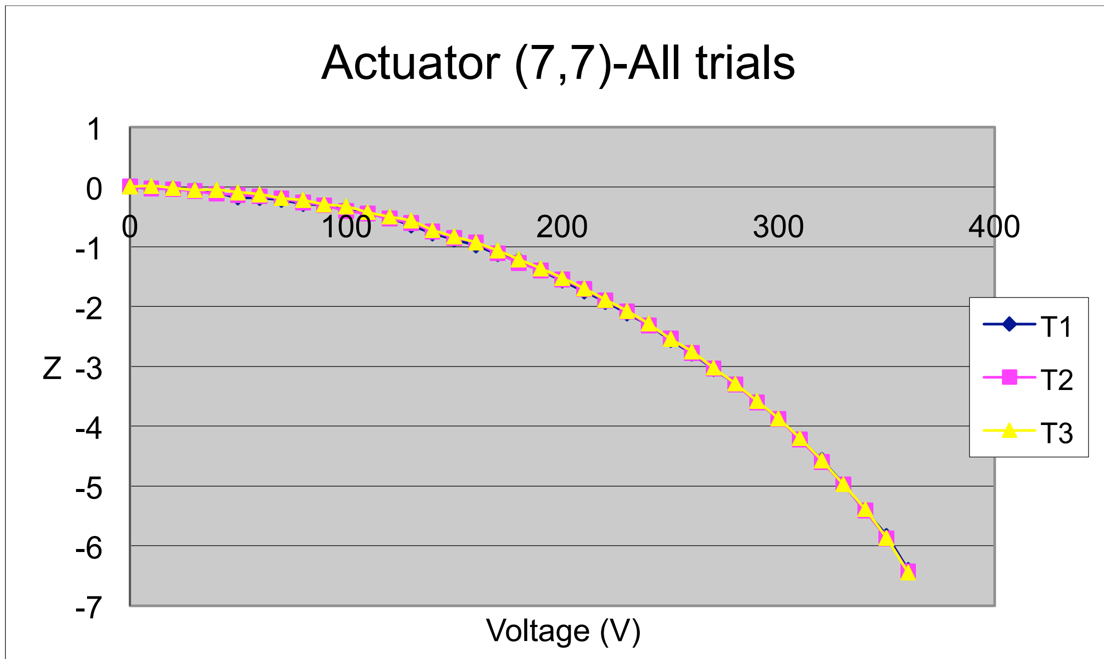

Figure 3.21: Repeatability of actuator (7,7) throughout the 3 trials

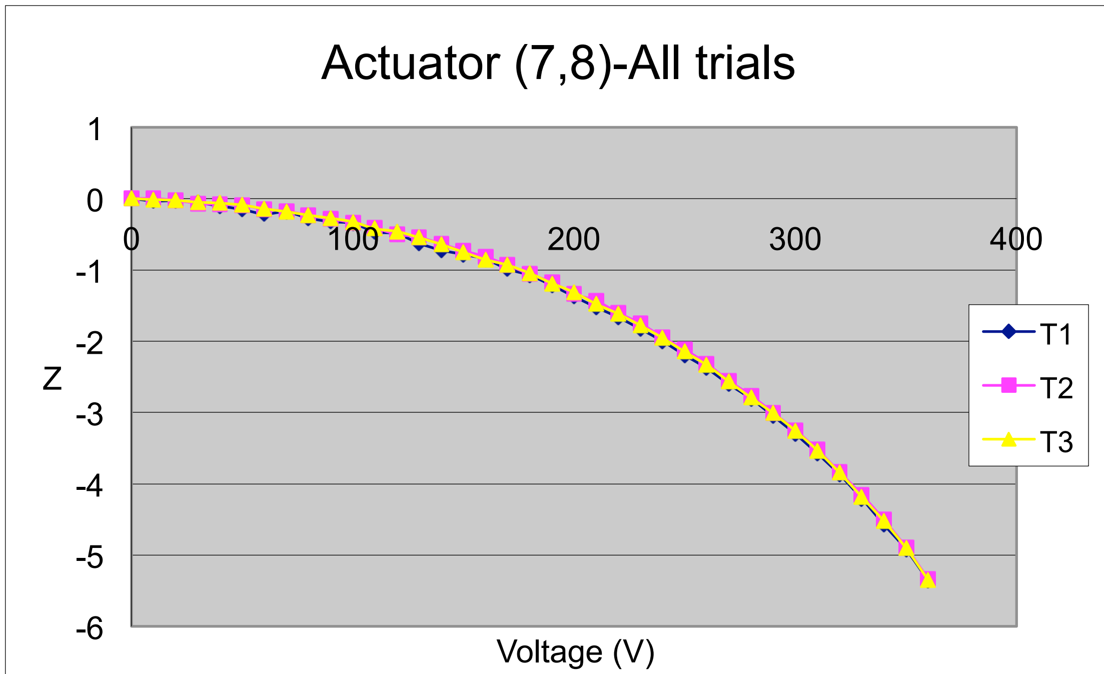

Figure 3.22: Repeatability of actuator (7,8) throughout the 3 trials

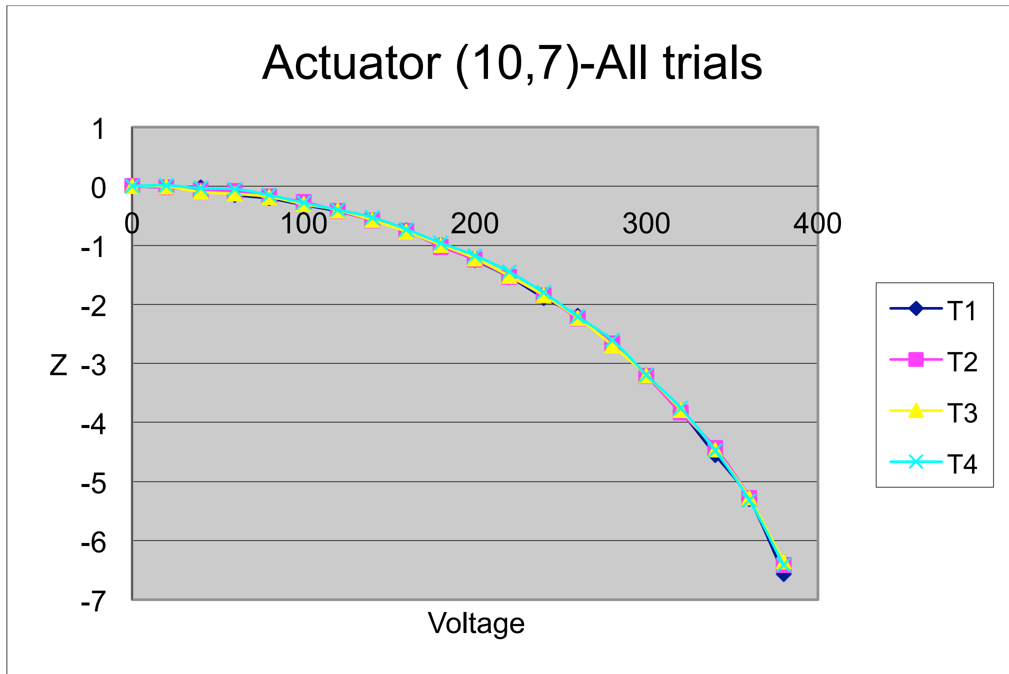

Figure 3.23: Repeatability of Actuator (10,7) throughout the four Trials

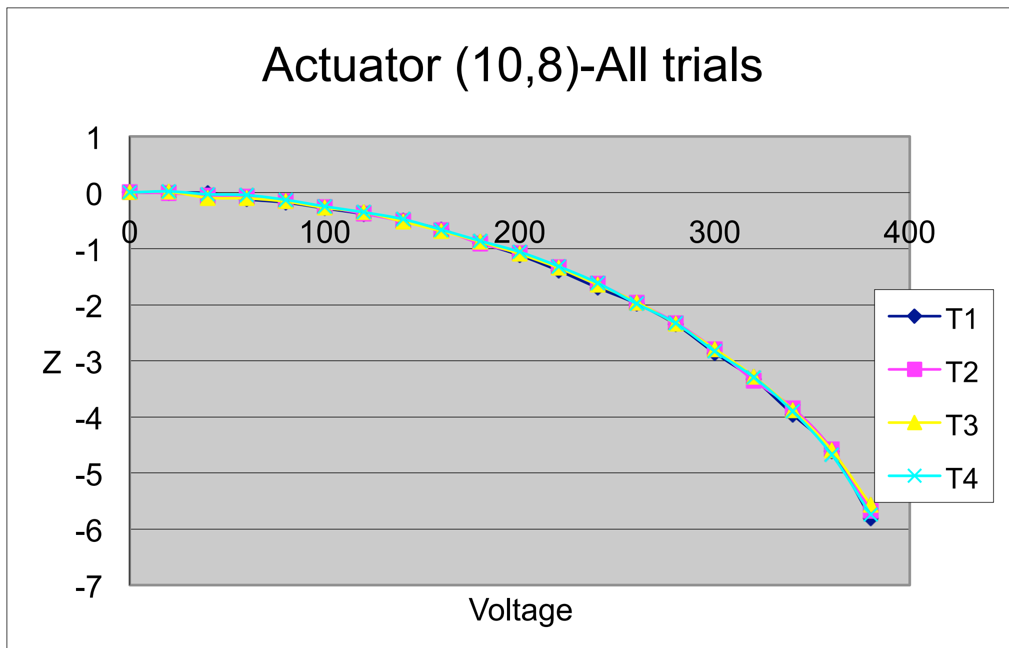

Figure 3.24: Repeatability of Actuator (10,8) throughout the four Trials

3.3 Summary/Discussion

Table (3.1) summarizes the maximum displacement of actuators (7,7) and (7,8) in pair actuator testing in all trials. Table (3.2) summarizes the maximum displacement of actuators (10,7) and (10,8) in pair actuator testing. Table (3.2) below compares the displacement between single and dual actuation for each actuator leading to the conclusion that the more actuators we use the less voltage we apply.

	Pair actuation displacement at 360 V Actuator (7,7) (μm)	Pair actuation displacement at 360 V Actuator (7,8) (μm)
Trial 1	6.4	5.36
Trial 2	6.42	5.33
Trial 3	6.45	5.35
Average	6.42	5.35

Table 3.1: The maximum displacement of actuators (7,7) and (7,8) in pair actuator testing in all trials

Actuator (7,7) reached 6.9 μm (basically 7 μm) at 370 V.

	Pair actuation displacement at 380 V Actuator (10,7) (μm)	Pair actuation displacement at 380 V Actuator (10,8) (μm)
Trial 1	6.56	5.80
Trial 2	6.41	5.67
Trial 3	6.35	5.57
Trial 4	6.41	5.74
Average	6.43	5.70

Table 3.2: The maximum displacement of actuators (10,7) and (10,8) in pair actuator testing in all trials

Actuator	Dual actuation Displacement (μm)	Single actuation Displacement (μm)
(7,7) at 360 V	6.42	4.15
(7,8) at 360 V	5.35	NA
(10,7) at 380 V	6.43	5.14
(10,8) at 380 V	5.70	4.58

Table 3.3: Comparison of the displacement between single and dual actuation for each actuator

From the tables above we can conclude that actuating multiple actuators we can achieve a higher stroke at lower voltage. However, not all of the actuators move to the same displacement under the same voltage. To understand this behavior the height of different actuators around this mirror was measured as shown in figure (3.25). On average we get 56.93 μm as the total thickness from the substrate to the mirror layer, 27.35 μm from the substrate to the spring layer and 0.25 μm for the counter electrode as shown in figure (3.26).

Mirror: 56.57 μm
Spring: 26.14 μm
Bottom Plate: NA

Mirror: 57.89 μm
Spring: 26.95 μm
Bottom Plate: 0.215 μm

Mirror: 59.44 μm
Spring: 27.66 μm
Bottom Plate: 0.012μm

Mirror:
54.88 μm
Spring:
26.73 μm
Bottom
Plate:
0.39μm

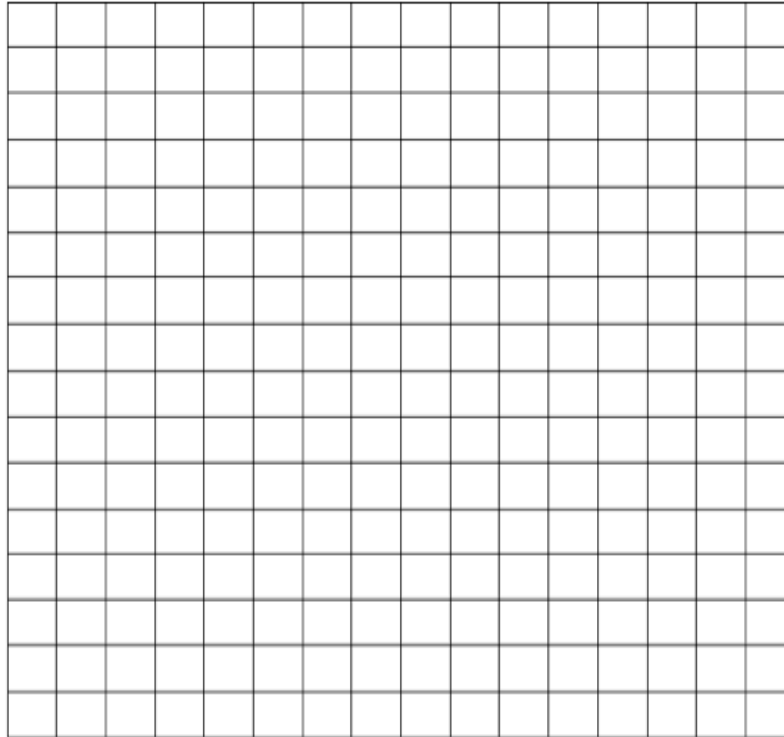

Mirror:
58.00 μm
Spring:
28.29 μm
Bottom
Plate:
0.134μm

Mirror: 55.06 μm
Spring: 26.9 μm
Bottom Plate: 0.27μm

Mirror: 56.6 μm
Spring: 27.65 μm
Bottom Plate: 0.44 μm

Mirror: 57.04 μm
Spring: 28.50 μm
Bottom Plate: 0.9643 μm

Figure 3.25: Height of actuators located in the corner of the deformable mirror as well as the height of actuators in the middle of each side of the mirror

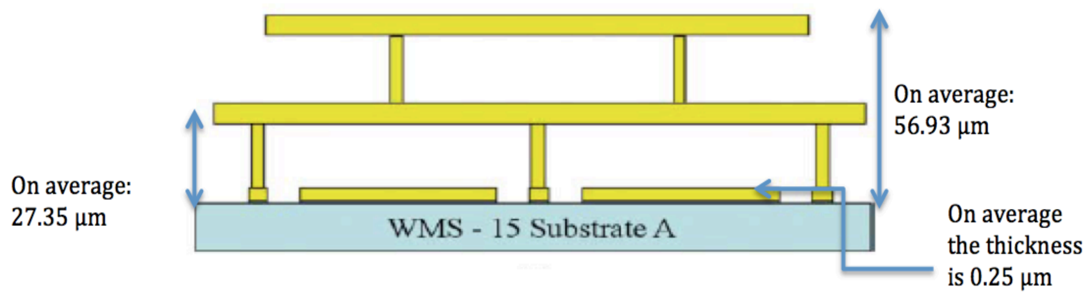

Figure 3.26: Average height from the substrate to the mirror layer, from the substrate to the spring layer and for the counter electrode of this deformable mirror

There are also bulls-eye test structures, as shown on figure (3.27), on two sides of this mirror: the right side and the bottom side. The heights of different layers of the bulls-eye were measured and summarized in table (3.4) below. On average, we get 0.44 µm for counter electrode, 22.493 µm for the gap between the counter electrode and the spring layer, 5.882 µm for spring layer, 25.3 µm for the post gap and 3.7 µm for the mirror layer leading to a total of 57.82 µm from the substrate to the mirror layer.

Location	Counter electrode	Gap	Spring layer	Post Gap	Mirror	Total
Right 1	0.47	22.49	6.31	24.28	5.94	59.48
Right 2	0.44	22.51	4.81	27.01	2.44	57.22
Right 3	0.36	22.65	5.57	28.25	1.35	58.19
Right 4	0.44	22.57	5.73	27.06	3.53	59.31
Right 5	0.42	22.66	5.74	24.92	3.46	57.20
Right 6	0.46	22.64	6.02	20.75	7.42	57.29
Right 7	0.48	22.57	5.72	27.39	1.10	57.27
Bottom 1	0.49	22.60	7.12	24.59	2.56	57.35
Bottom 2	0.41	22.51	5.25	26.87	2.44	57.49
Bottom 3	0.44	22.39	6.44	23.80	3.96	57.03
Bottom 4	0.45	22.27	5.36	25.82	5.80	59.70
Bottom 5	0.42	22.06	6.51	22.90	4.38	56.27
Average	0.44	22.49	5.88	25.30	3.70	57.82

Table 3.4: Summary of the heights of the counter electrode, the gap between the counter electrode and spring layer, the post gap, the mirror layer and the total height of each bulls-eye that are part of the DM.

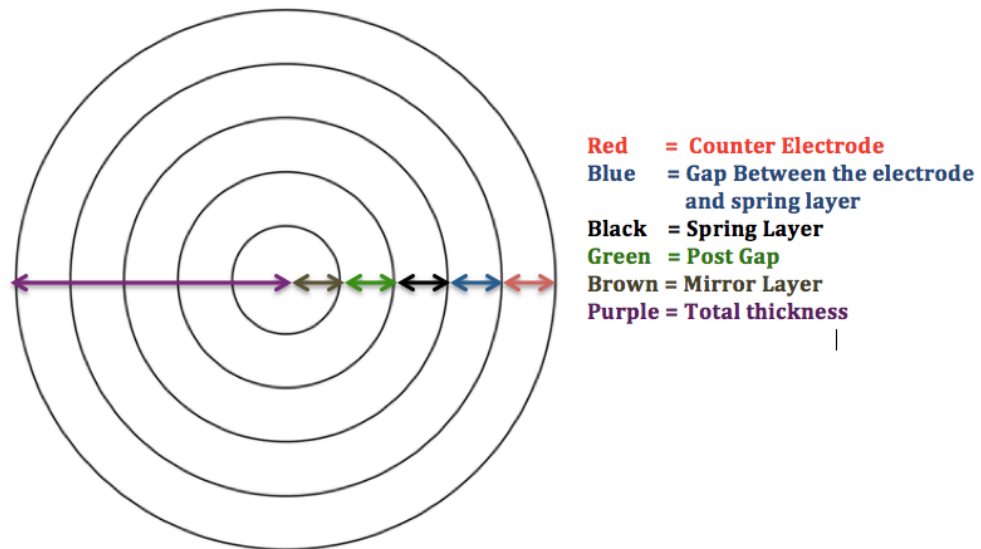

Figure 3.27: An illustration of a test-structure (bulls-eye) found around the mirror

The heights of different layers of test structures (bulls-eye) that are not part of the mirror were also measured for comparison as shown in tables (3.5) and (3.6) below.

Location	Counter electrode	Gap	Spring layer	Post Gap	Mirror	Total
1	0.35	20.26	2.85	24.89	1.36	49.72
2	0.41	20.66	1.83	25.04	1.55	49.49
3	0.39	20.85	3.58	24.30	3.67	52.79
4	0.42	21.05	2.84	24.75	6.34	55.39
5	0.43	21.15	2.98	26.29	3.78	54.63
6	0.44	21.41	3.65	27.77	1.50	54.77
7	0.43	21.75	4.07	24.07	5.50	55.81
8	0.41	21.79	4.21	25.15	4.91	56.48
9	0.42	21.91	4.46	27.88	2.21	56.88
10	0.42	21.97	4.86	27.97	2.46	57.68
11	0.40	22.04	4.56	26.01	3.61	56.62
12	0.43	22.01	4.75	26.55	3.49	57.23
13	0.43	21.95	4.94	28.27	1.91	57.49
14	0.43	21.88	4.56	26.26	3.48	56.61
15	0.39	21.93	4.57	26.52	3.58	56.99
16	0.41	21.66	4.53	28.26	1.85	56.71
17	0.42	21.59	4.54	26.70	3.50	56.74
18	0.39	21.46	4.09	26.76	3.07	55.77
19	0.41	20.75	3.86	26.27	3.41	54.70
20	0.40	20.52	3.20	27.56	2.52	54.20
21	0.42	19.81	2.04	24.33	5.80	52.40
22	0.42	19.45	1.46	25.23	3.10	49.66
23	0.43	19.34	1.85	27.05	4.56	53.24
Average	0.41	21.18	3.67	26.25	3.35	54.87

Table 3.5: Summary of the heights of the counter electrode, the gap between the counter electrode and spring layer, the post gap, the mirror layer and the total height of bulls-eyes that are not part of the mirror.

If we compare the average heights between the test structures on the mirror with the others that are not on the mirror we can see that there is a discrepancy in the height of the spring layer of approximately 2µm, a discrepancy of 3µm in the mirror layer and a discrepancy of 1.2µm in the gaps. These discrepancies lead to the conclusion that actuators throughout the mirror do no necessarily have the same gap between the counter electrode and the spring layer, thus explaining why some actuators achieve higher stroke than others.

Location	Counter electrode	Gap	Spring layer	Post Gap	Mirror	Total
DM	0.44	22.49	5.88	25.30	3.70	57.81
OFF DM	0.41	21.18	3.67	26.25	3.35	54.87

Table 3.6: Comparison between the heights of the counter electrode, the gap between the counter electrode and spring layer, the post gap, the mirror layer and the total height of bulls-eyes that are part of the DM and ones that are not part of the DM.

In order to reach 10 µm of stroke and avoid breakdown more than two actuators must be actuated at the same time. According to the modified Paschen curve we can apply approximately 400 V for a 20 µm gap, between the counter electrode and the spring layer, before we reach breakdown as shown in figure (3.7). This graph also gives the safe operating region for operating MEMS device, which in between 360 – 370 V [10].

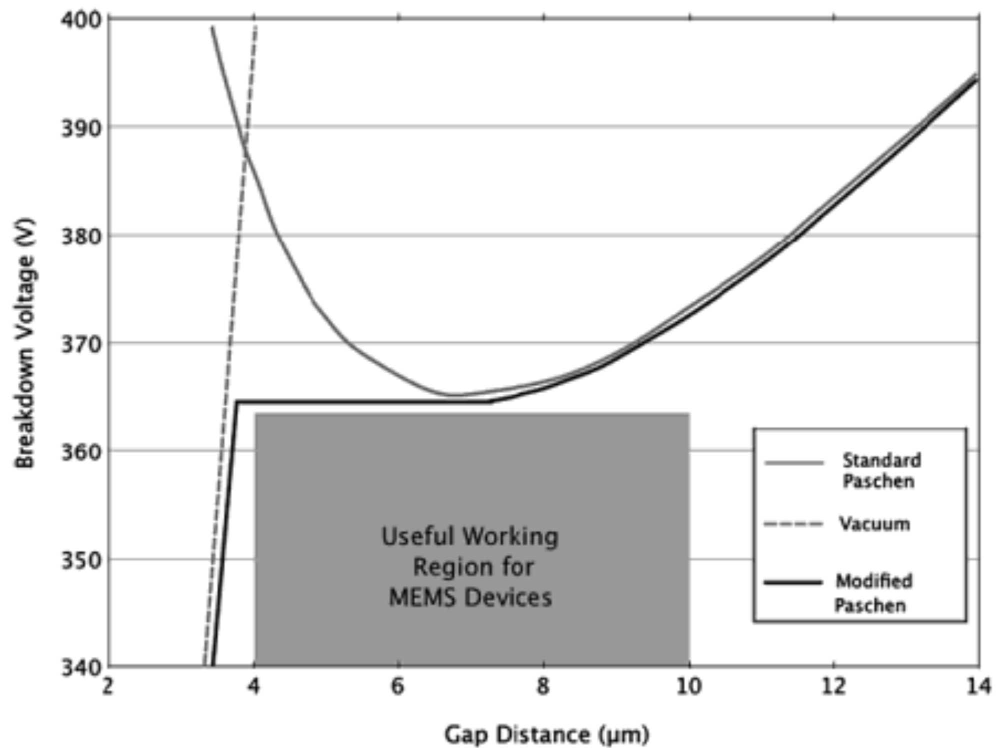

Figure 3.28: Standard Paschen curve, modified Paschen curve, Vacuum breakdown, and safe operating region for MEMS for air at one atmosphere [10]

Unfortunately we cannot use actuators (7,7), (7,8), (10,7) and (10,8) for 2 x 2 actuator testing because they are far apart. Directly between them there is a hole, preventing further testing in that region.

Chapter 4: Future Work

4.1 Individual Actuator Testing

In order to perform 2 x 2 testing, a second 16 x 16 X-beam actuators deformable mirror is in the process of being tested. Figure (4.1) shows an image of the center 4 x 4 actuators of this mirror. A displacement of 1.4 µm on average is achieved at a maximum voltage of 280 V. This displacement is basically 1 µm less than the previous mirror discussed above in this thesis at the same voltage. Preliminary individual testing of the 16 x 16 X-beam deformable mirror showed that 13 out of the 16 4 x 4 center actuators are more or less behaving as expected. The graphs below show the average displacement of each actuator from 0 to 280 V for 13 actuators of the center 4 x 4 as shown in figures (4.2), (4.3), (4.4) and (4.5). We can therefore conduct dual, 2 x 2 and eventually 4 x 4 testing and see how much displacement we can achieve.

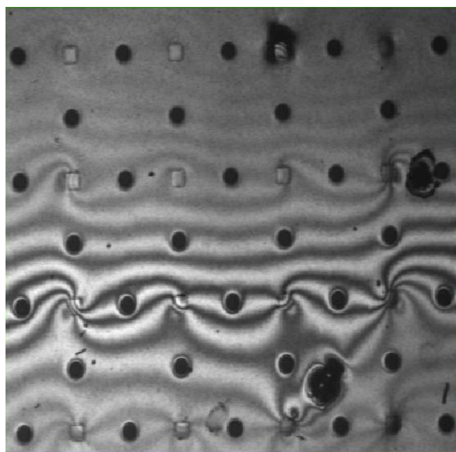

Figure 4.1: Image of the Center 4 x 4 X-Beam Actuators of second DM

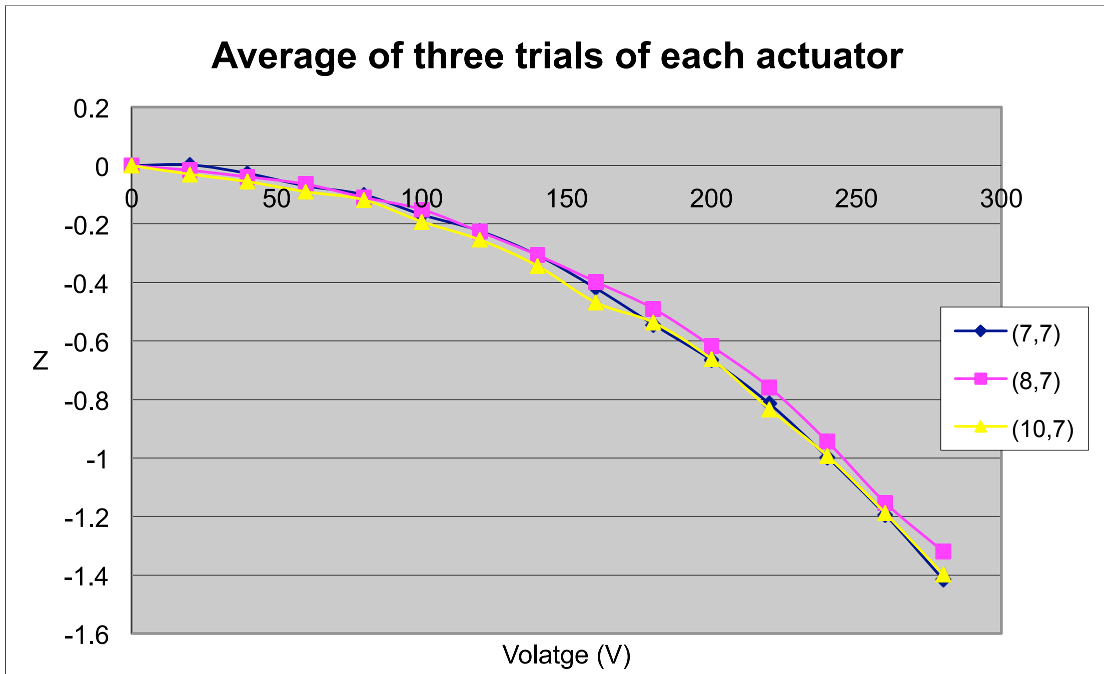

Figure 4.2: Graph of the average displacement of actuator (7,7), (8,7) and (10,7) from 0 to 280 V for the top row of the center 4 x 4

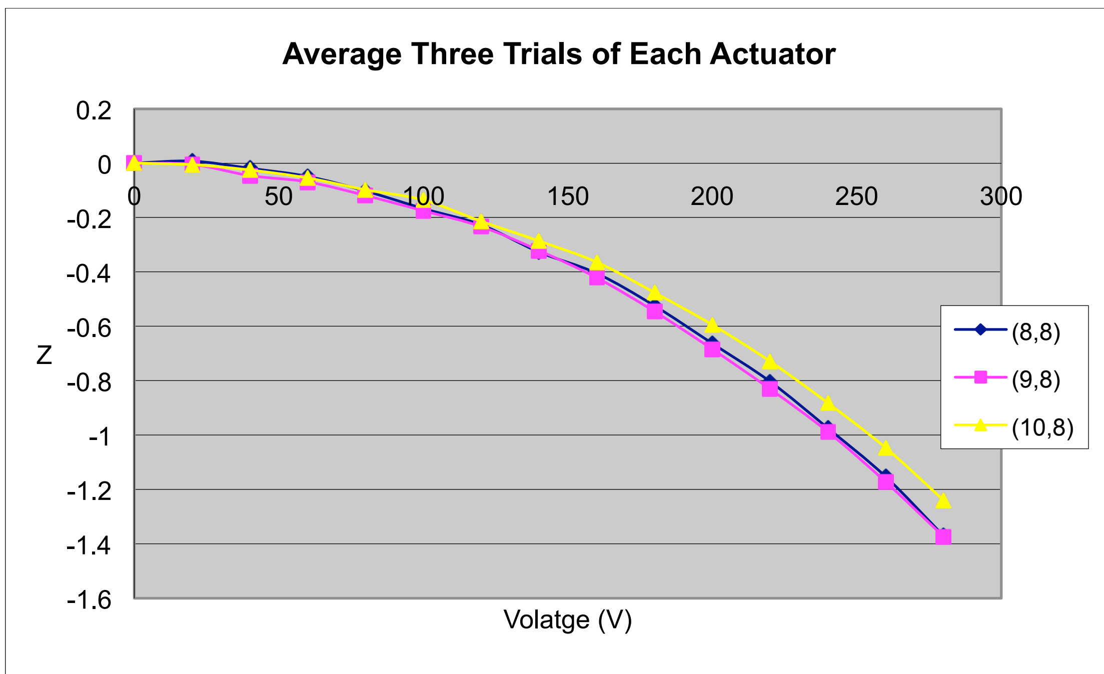

Figure 4.3: Graph of the average displacement of actuator (8,8), (9,8) and (10,8) from 0 to 280 V for the second row of the center 4 x 4

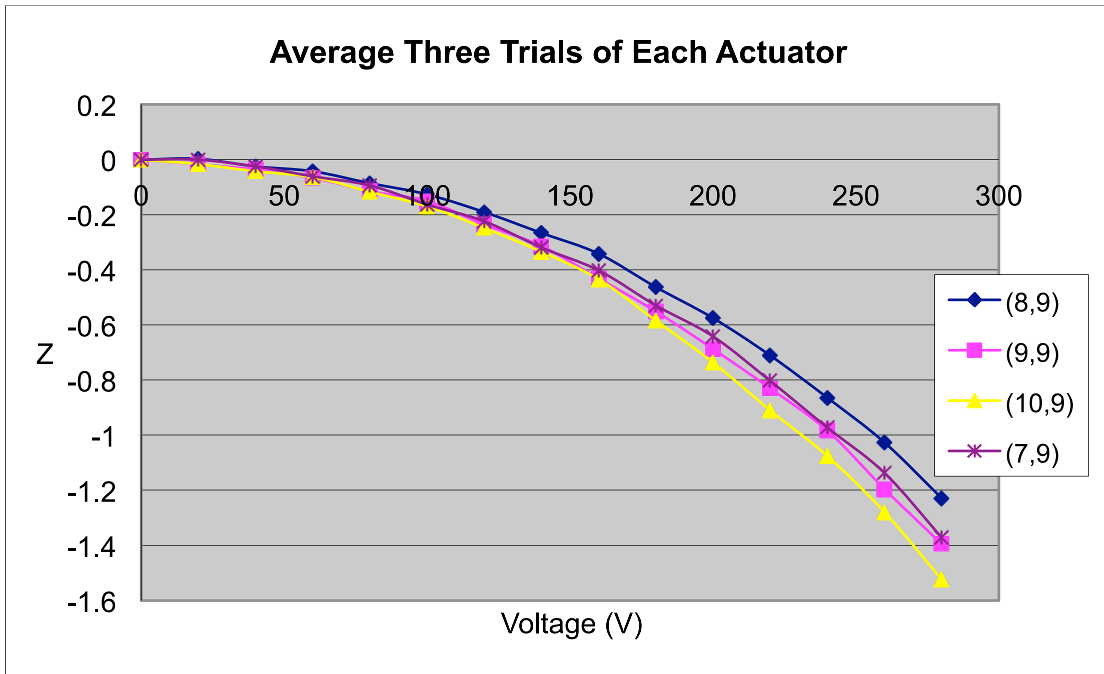

Figure 4.4: Graph of the average displacement of actuator (7,9), (8,9), (9,9) and (10,9) from 0 to 280 V for the third row of the center 4 x 4

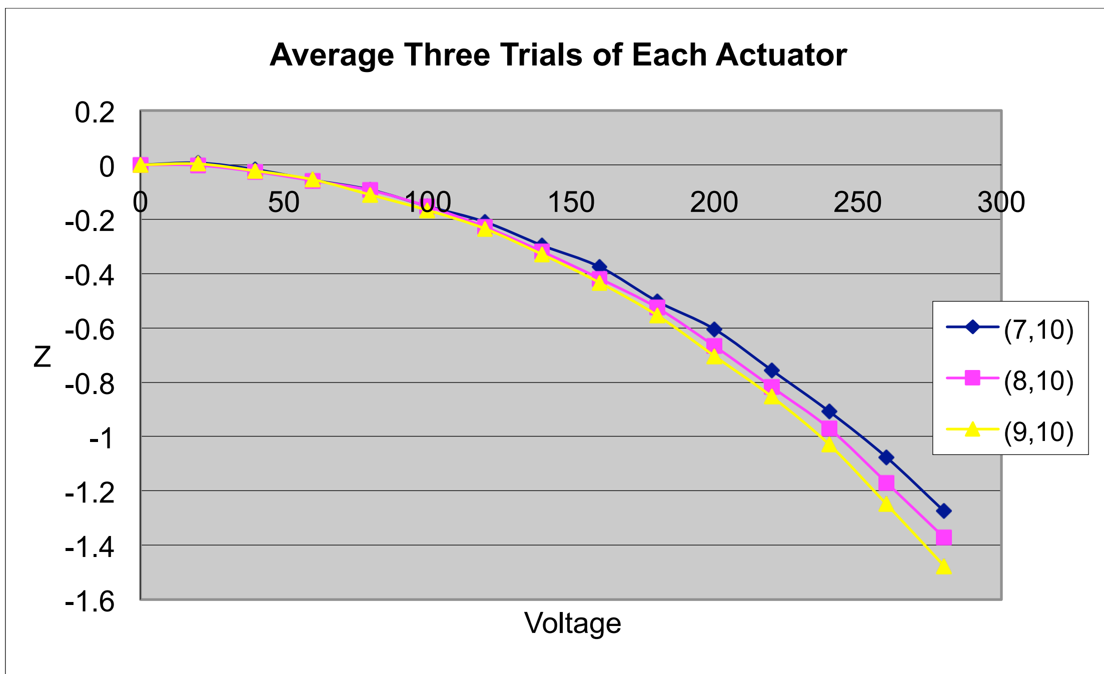

Figure 4.5: Graph of the average displacement of actuator (7,10), (8,10), and (9,10) from 0 to 280 V for the bottom row of the center 4 x 4

4.2 Dual Actuators Testing

The second mirror's dual testing have shown that the center 4 x 4 x-beam actuators are behaving as expected; the more voltage applied the more displacement achieved as shown in the figures below. Also, these results show that the more actuators are tested at the same time the less voltage applied, which is similar to the behavior of the first DM tested. In addition, this graphs show that the behavior of these actuators is also repeatable in the four trials conducted for each actuator. However, the maximum displacement achieved in dual actuator testing is only 4.5µm at 360 V for actuator (7,7) compared to the same actuator of the first mirror.

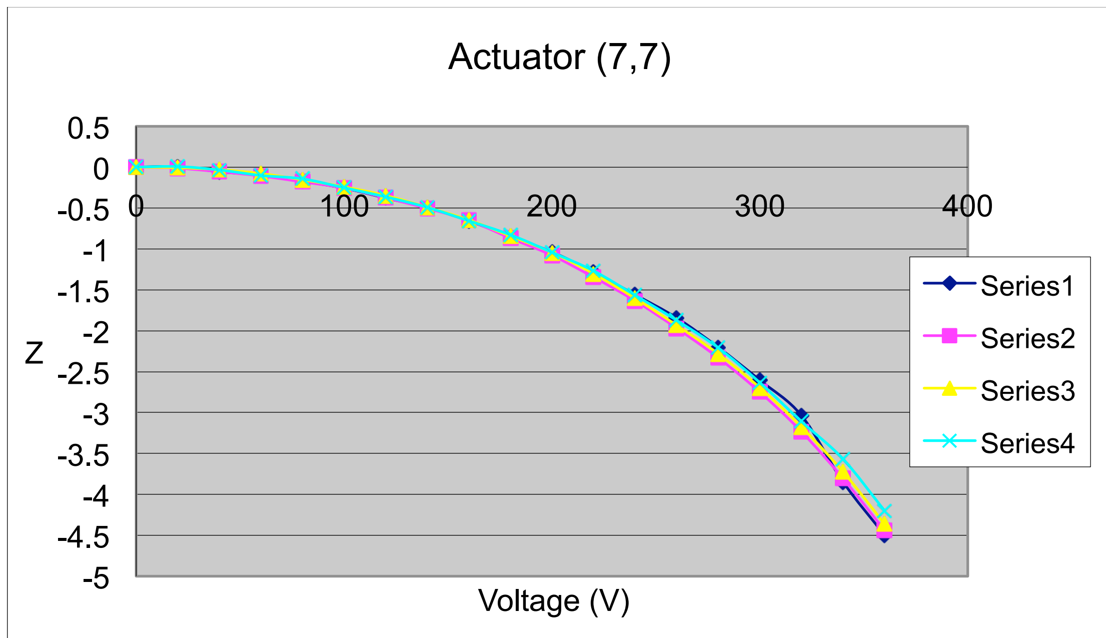

Figure 4.6: Repeatability of Actuator (7,7) throughout the four Trials of dual actuator testing of the second DM

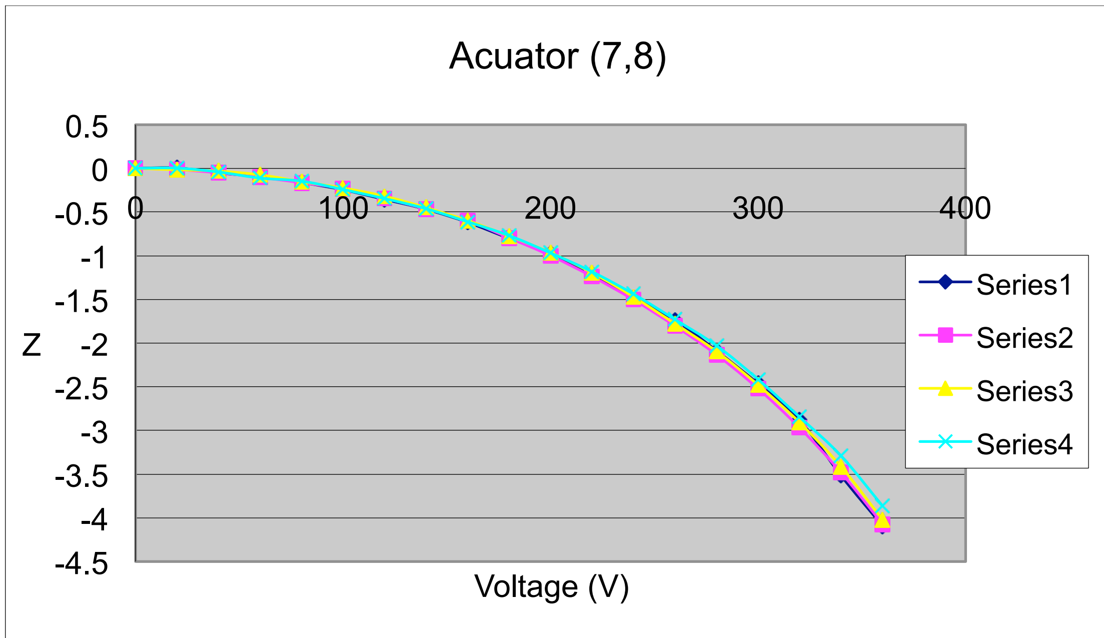

Figure 4.7: Repeatability of Actuator (7,8) throughout the four Trials of dual actuator testing of the second DM

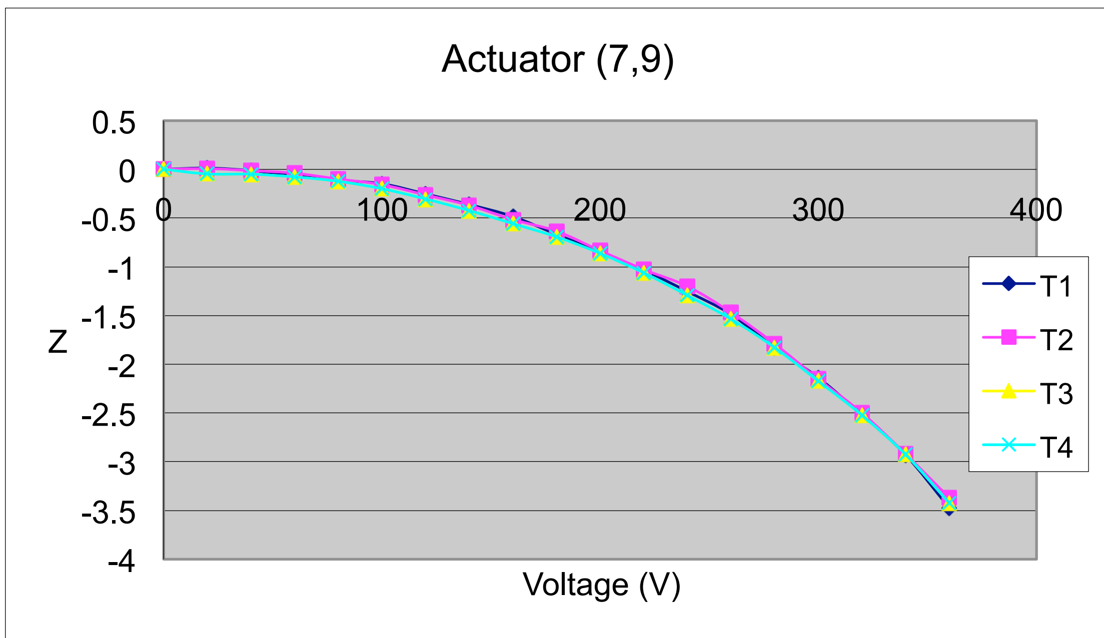

Figure 4.8: Repeatability of Actuator (7,9) throughout the four Trials of dual actuator testing of the second DM

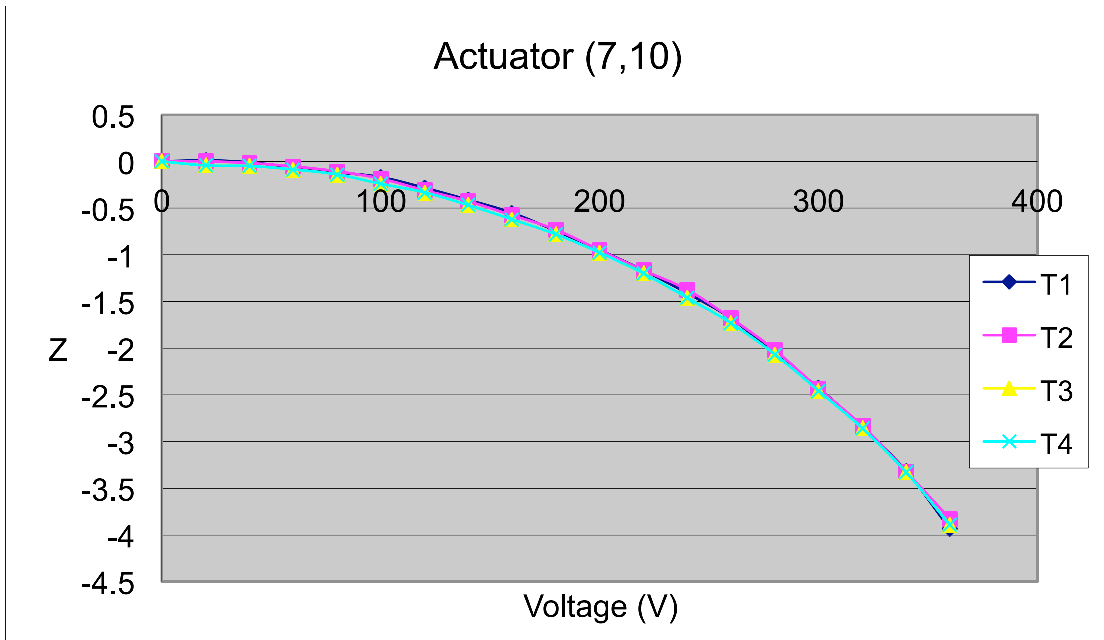

Figure 4.9: Repeatability of Actuator (7,10) throughout the four Trials of dual actuator testing of the second DM

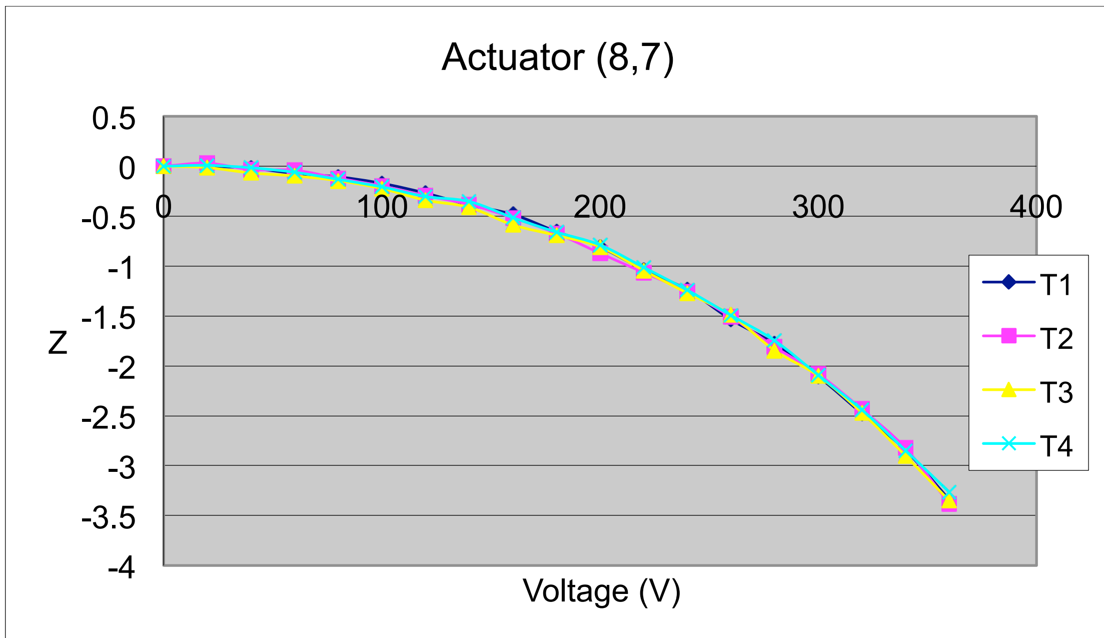

Figure 4.10: Repeatability of Actuator (8,7) throughout the four Trials of dual actuator testing of the second DM

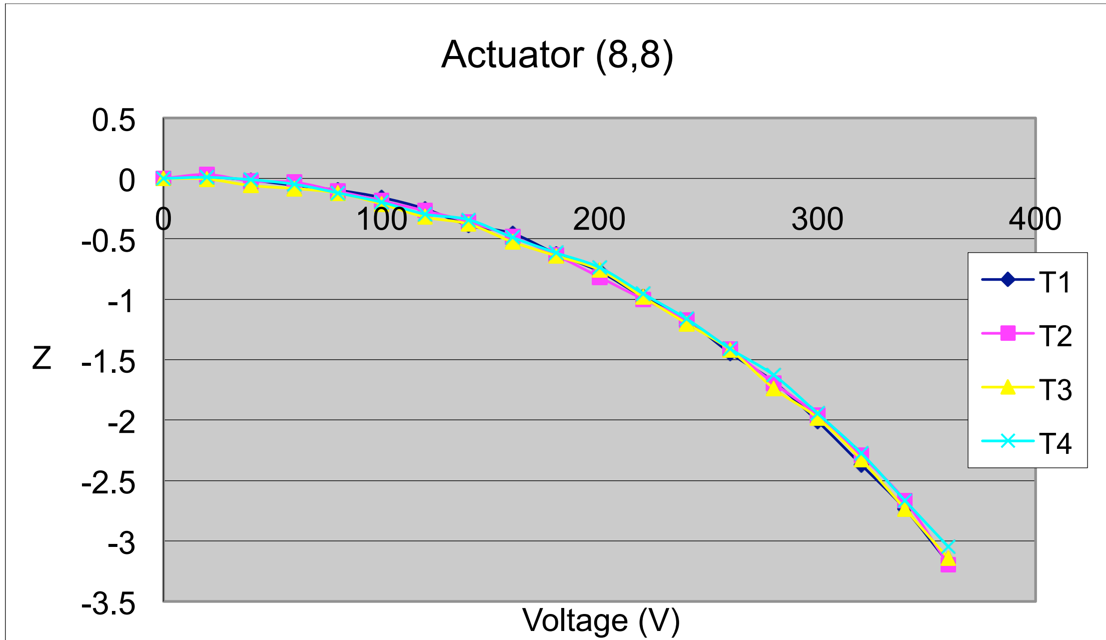

Figure 4.11: Repeatability of Actuator (8,8) throughout the four Trials of dual actuator testing of the second DM

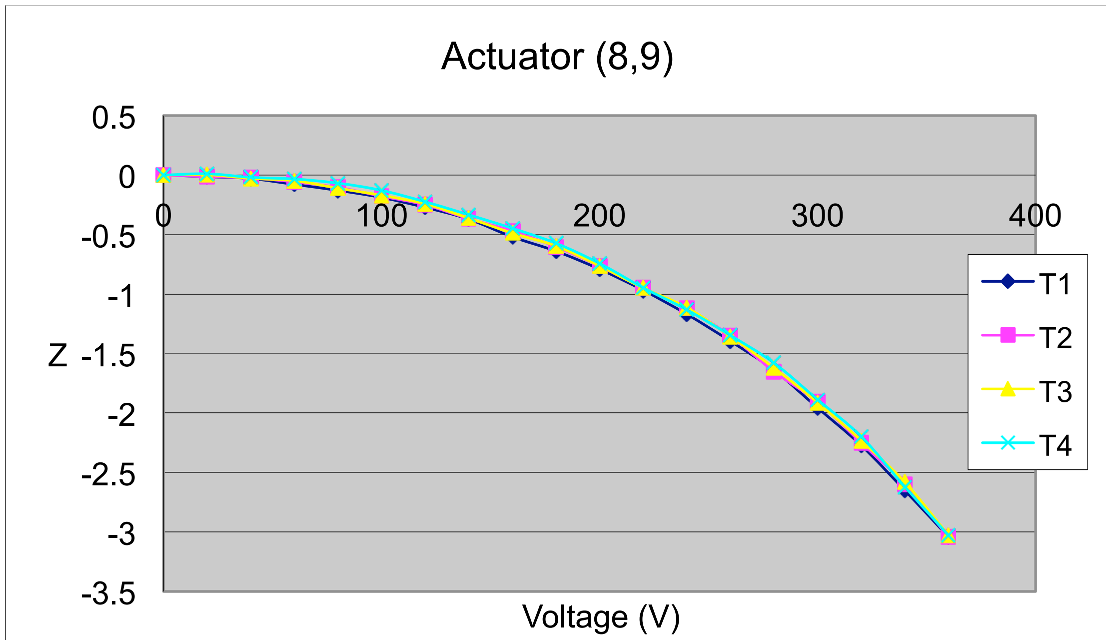

Figure 4.12: Repeatability of Actuator (8,9) throughout the four Trials of dual actuator testing of the second DM

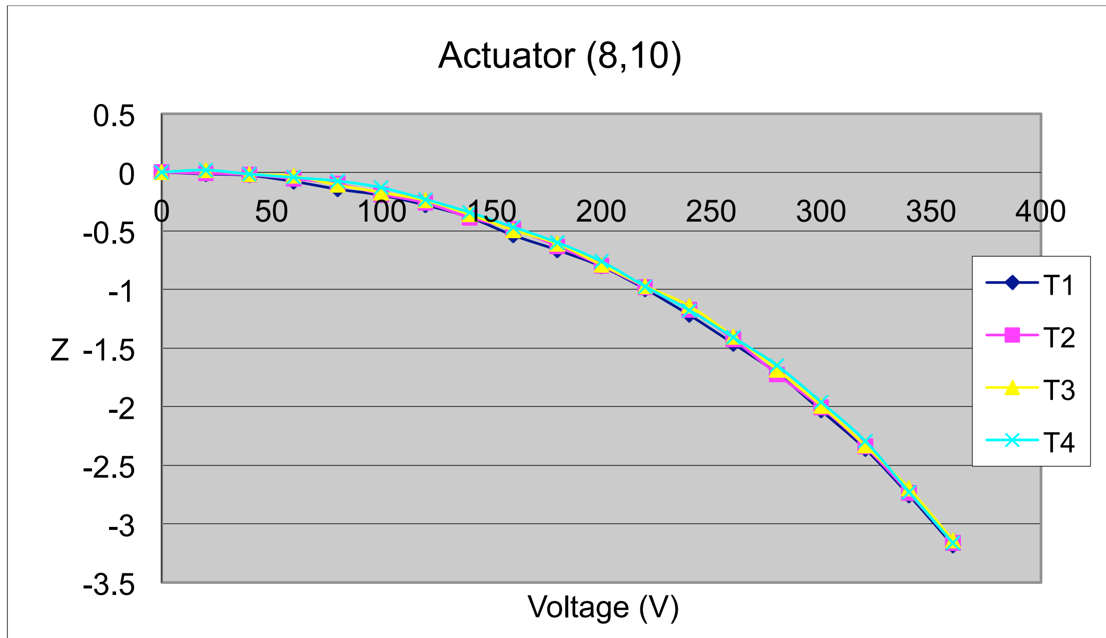

Figure 4.13: Repeatability of Actuator (8,9) throughout the four Trials of dual actuator testing of the second DM

4.3 Future Work

The second mirror's actuators are following the similar trend compared to the first mirror's actuators. Therefore, 2 x 2 and 4 x 4 actuators testing of the second DM is in the process to achieve higher stroke than 4.5 μm realized in the dual actuating testing.

If the center 4x4 actuators behave as expected then the next step in testing the mirrors would require a bigger actuator test area. A new PCB would be planned that will allow the use of a current commercial deformable mirror power supply from Boston Micro-machines Corporation (BMC) to actuate the

deformable mirrors actuators at different voltages. The voltage output of the BMC power supply will be summed to a constant voltage to allow a high voltage (+300V) to be applied to each actuator. The testing will be performed on the central 4×4 and eventually expanded to the entire central 12×12 actuators.

Conclusion

Micro-Electro-Mechanical System (MEMS) X-beam actuators deformable mirrors were fabricated using high-aspect ratio monolithic process by Innovative Micro Technology. This process was used to fabricate 16 x 16 X-beam actuators deformable mirrors and individual and dual actuator testing has been conducted.

Thorough characterization testing was performed on the fabricated MEMS deformable mirrors. The Veeco WYKO NT1100 White Light Interferometer was used to perform stroke measurements while the data was collected in the WYKO Vision 32 Software for further analysis.

Single actuator testing achieved approximately a maximum of 5.14µm for actuator (10,7) while dual actuator testing achieved a maximum of approximately 7µm for actuator (7,7) for the first deformable mirror. These results show that applying voltage to multiple actuators achieves a higher stroke at lower voltage. In addition, the data show the repeatability of these actuators' voltage vs. displacement curve as expected.

These results lead to the conclusion that the high aspect ratio monolithic fabrication process is capable of the fabrication of high stroke MEMS deformable mirrors that are suitable for the next generation of telescopes. In addition, these mirrors hold great promise for applications in vision science that requires a stroke of 15 µm.

Bibliography

1) Dr. Claire Max, Center for Adaptive Optics, University of California, Santa Cruz

2) Thomas Bifano, Paul Bierden, and Julie Perreault, Micromachined Deformable Mirrors for Dynamic Wavefront Control, Proc. SPIE 5553, pp. 10-13 (2004).

3) Joel A. Kubby, A Guide to Hands-on MEMS Design and Prototyping, Cambridge University Press, (2011).

4) Joel Kubby, Adaptive Optics for Biological Imaging, Taylor & Francis, CRC Press.

5) Bautista R. Fernández and Joel Kubby, High-aspect ratio microelectromechanical systems deformable mirrors for adaptive optics, J. Micro/Nanolitho. MEMS MOEMS 9, pp. 041106 (2010).

6) Bautista Fernández Rocha, Design, Fabrication and Characterization of High-Stroke High-Aspect Ratio Micro Electro Mechanical Systems Deformable Mirrors For Adaptive Optics, PhD Thesis, University of California Santa Cruz, Dept. of Electrical Engineering (2011).

7) E. S. Hung and S. D. Senturia, "Extending the travel range of analog tuned electrostatic actuators," *Journal of Microelectromechanical Systems* 8, 497–505 (1999).

8) Veeco. "NT1100 Setup Guide".

9) Geoff Andersen, The Telescope- Its History, Technology, and Future, Princeton University Press, New Jersey, pp 44 – 139 (2006).

10) Allyson L. Hartzell, Herbert R. Shea, MEMS Reliability, Springer, (2011)